

# NASA CONTRACTOR REPORT

NASA CR-2824



NASA CR-2

0061697



TECH LIBRARY KAFB, NM

LOAN COPY: RETURN TO  
AFWL TECHNICAL LIBRARY  
KIRTLAND AFB, N. M.

## SUMMARY REPORT OF EVALUATION OF COATED COLUMBIUM ALLOY HEAT SHIELDS FOR SPACE SHUTTLE THERMAL PROTECTION SYSTEM APPLICATION

*W. E. Black*

*Prepared by*  
CONVAIR DIVISION OF GENERAL DYNAMICS  
San Diego, Calif. 92123  
*for Langley Research Center*



0061697

1. Report No. NASA CR-2824		2. Government Accession No.		3. Recipient's Catalog No.	
4. Title and Subtitle Summary Report of Evaluation of Coated Columbium Alloy Heat Shields for Space Shuttle Thermal Protection System Application				5. Report Date April 1977	
				6. Performing Organization Code	
7. Author(s) W. E. Black				8. Performing Organization Report No. CASD-NAS-76-056	
9. Performing Organization Name and Address Convair Division of General Dynamics 5001 Kearny Villa Road, San Diego, CA 92123				10. Work Unit No.	
				11. Contract or Grant No. NAS1-9793	
12. Sponsoring Agency Name and Address NASA Langley Research Center, Materials Division, Materials Research Branch, Hampton, Virginia				13. Type of Report and Period Covered Contractor 10-70 to 3-74	
				14. Sponsoring Agency Code	
15. Supplementary Notes D. R. Rummler was the NASA technical monitor. <span style="float: right;">Final Report</span>					
16. Abstract This report summarizes a three-phase program to develop and demonstrate the feasibility of a metallic heat shield suitable for use on Space Shuttle Orbiter class vehicles at operating surface temperatures of up to 1590 K (2400°F). An orderly progression of configuration studies, material screening tests, and subscale structural tests was performed. Scale-up feasibility was demonstrated in the final phase when a sizeable nine-panel array was fabricated and successfully tested. The full-scale tests included cyclic testing at reduced air pressure to 1590 K (2400°F) and up to 158 dB overall sound pressure level. Earlier testing had verified the suitability of the design and the selected coated columbium alloy system (Cb-752/R-512E) to withstand expected micrometeoroid particle impact and lightning strike damage. Tensile and creep data under both isothermal and cyclic conditions were gathered to provide a basis for future structural applications. The selected structural configuration and design techniques successfully eliminated thermal induced failures. The thermal/structural performance of the system was repeatedly demonstrated during the program. Practical and effective field repair methods for coated columbium alloys were demonstrated. Major uncertainties of accessibility, refurbishability, and durability were eliminated. The final system design had a unit weight (including heat shield, retainers, insulation, and supporting structure) of 23 kg/m <sup>2</sup> (4.7 lb/ft <sup>2</sup> ) and a unit cost of \$1100/kg (\$500 lb). Projections for a five-shipset procurement reduced the unit cost to \$580/kg (\$265/lb).					
17. Key Words (Suggested by Author(s)) Columbium alloys, Space Shuttle Orbiter, heat shields, thermal protection system				18. Distribution Statement Unclassified- Unlimited  Subject Category 39	
19. Security Classif. (of this report) Unclassified		20. Security Classif. (of this page) Unclassified		21. No. of Pages 65	22. Price \$4.50



# CONTENTS

	Page
INTRODUCTION . . . . .	1
MODEL VEHICLE AND ENVIRONMENT . . . . .	3
HEAT SHIELD CONFIGURATION STUDY . . . . .	4
TPS DESIGN . . . . .	9
ELEMENTAL SPECIMEN TESTING . . . . .	11
RESIDUAL MECHANICAL PROPERTIES . . . . .	13
MICROMETEOROID IMPACT TESTS . . . . .	14
Erosion Tests . . . . .	15
Cratering Tests . . . . .	15
Perforation Tests . . . . .	16
LIGHTNING STRIKE TESTS . . . . .	19
SUBSIZE TPS PANELS . . . . .	22
Panel Fabrication . . . . .	22
Panel Testing . . . . .	25
SMALL SIZE TPS HARDWARE FABRICATION . . . . .	27
SMALL-SIZE TPS TESTING . . . . .	31
Thermal Flow Testing . . . . .	31
Open corrugation TPS . . . . .	31
Tee-stiffened TPS . . . . .	33
Hot gas flow test summary . . . . .	33
Radiant Heat Testing . . . . .	35
Open corrugation TPS . . . . .	35
Tee-stiffened TPS . . . . .	35
Radiant heat test summary . . . . .	36
Acoustic Testing . . . . .	37
FULL-SIZE TPS . . . . .	37
Testing . . . . .	38
Pre-thermal acoustic testing . . . . .	39
Thermal-mechanical testing . . . . .	39
Thermal-mechanical test results . . . . .	44
Thermal correlation . . . . .	46
Post-thermal acoustic testing . . . . .	49
Test Evaluation . . . . .	49
Specimen disassembly . . . . .	49
Thermal/structural performance . . . . .	49

	Page
TPS WEIGHT ASSESSMENT . . . . .	51
TPS COST ASSESSMENT . . . . .	52
CONCLUDING REMARKS . . . . .	54
APPENDIX A . . . . .	57
REFERENCES . . . . .	61

## FIGURES

		Page
1	The Metallic TPS Concept . . . . .	2
2	Predicted Orbiter Maximum Surface Temperature . . . . .	3
3	Selected Area of Investigation . . . . .	3
4	Design and Test Profile . . . . .	4
5	Open-Corrugated TPS Exploded Assembly . . . . .	10
6	Ultimate Strength of Cb-752/R-512E After 100 Cycles . . . . .	14
7	Yield Strength of Cb-752/R-512E After 100 Cycles . . . . .	14
8	Creep Properties of Cb-752/R-512E at 1370 K (2000° F), 1480 K (2200° F) and 1590 K (2400° F) . . . . .	14
9	Columbium Alloy Coupons after Bombardment and Thermal Exposure . . . . .	17
10	Pre-Oxidized Cb-752/R-512E Test Specimen after Lightning Strike Test Sequence . . . . .	21
11	Exterior View of As-Coated Unexposed Subsize Corrugated Panel . . . . .	23
12	Interior View of As-Coated Unexposed Subsize Tee-Stiffened Panel . . . . .	23
13	Fabrication Sequence for Subsize TPS Panels . . . . .	24
14	Subsize Tee-Stiffened Panel Fabrication Sequence . . . . .	25
15	Exterior View of Cb-752/R-512E Tee-Stiffened Subsize Panel after 100 Flight Simulation Cycles . . . . .	28
16	Exterior View of Cb-752/R-512E Open Corrugation Subsize Panel after 100 Flight Simulation Cycles . . . . .	28
17	Interior View of Brazed Cb-752 Open Corrugation Heat Shield . . . . .	29
18	Interior View of Electron Beam Welded Tee-Stiffened Cb-752 Heat Shield . . . . .	30
19	Open Corrugation TPS Specimen Installed in Hot Gas Flow Facility Prior to Testing . . . . .	32
20	Hot Gas Flow Test Composite Temperature Distribution — Open Corrugation TPS . . . . .	33

	Page
21 Unexposed Tee-Stiffened TPS Specimen — End View . . . . .	34
22 Tee-Stiffened Heat Shield (Exterior Side) and Attachments after 20 Hot Gas Flow Thermal Cycles and 100 Acoustic Cycles . . . . .	34
23 Tee-Stiffened TPS Specimen after 50 Radiant Heat/Pressure/Load Cycles — Side View . . . . .	36
24 Assembled Test Specimen Prior to Testing . . . . .	40
25 Acoustic Spectrum — High Level (Pre-Thermal Tests) . . . . .	41
26 Facility for Thermal, Load, and Environmental Testing of Multi-Panel TPS . . . . .	42
27 Schematic for Multi-Panel TPS Test Facility . . . . .	43
28 Test Parameters for Nine-Panel Test Specimen . . . . .	44
29 Nine-Panel TPS Specimen after 50 Cycles of Thermal Flight Simulation .	45
30 Radiant Heat Test Composite Temperature Distribution . . . . .	47
31 Disassembled Nine-Panel TPS Specimen Components after 50 Thermal and 100 Acoustic Life Cycle Tests . . . . .	50
32 Panel after Testing . . . . .	50
33 Tee-Stiffened TPS Cumulative Average Cost . . . . .	53

TABLES

I Heat Shield Configuration Evaluation . . . . .	5
II Heat Shield Concept Summary . . . . .	7
III Columbium Alloy Heat Shield Configuration Selection . . . . .	8
IV Flight Simulation Test Results for Elemental Specimens . . . . .	12
V Nominal Applied Stress Levels for Subsize Panels . . . . .	26
VI Flight Simulation Test Summary for Subsize Panels . . . . .	27
VII TPS Weight Summary . . . . .	52
VIII Final TPS Fabrication Process Percentage Cost Breakdown . . . . .	53

SUMMARY REPORT OF EVALUATION OF COATED  
COLUMBIUM ALLOY HEAT SHIELDS FOR SPACE SHUTTLE  
THERMAL PROTECTION SYSTEM APPLICATION

By W. E. Black  
Convair Division of General Dynamics  
San Diego, California

INTRODUCTION

One key element in the success of reusable orbital vehicles is the thermal protection system (TPS). It must be capable of withstanding the imposed structural loads as well as dissipating heat generated by aerodynamic friction. One promising TPS concept from a reliability, inspection, cost, and reusability standpoint is a metallic radiative heat shield fabricated from suitable, coated columbium alloys.

A logical sequence of analytical and experimental investigations involving simulated mission and environmental conditions was followed to evaluate and demonstrate the feasibility of a coated columbium alloy TPS system.

Figure 1 describes the elements of a metallic heat shield by illustrating the final panel design. The exterior of the vehicle is covered by a series of these panels shingled in the direction of flow. The heat shield panel receives the full heat flux and aerodynamic pressure experienced by the vehicle. Most of the surface heat is radiated away from the heat shield. The fibrous insulation prevents excessive substructure heating, but it is not required to sustain airloads. The support posts provide a direct load path between the primary structure and the heat shields. The posts have a small cross sectional area; consequently, little heat is conducted through them to the substructure. The insulation retains heat collected during reentry and continues to heat the substructure for some time after the peak heat shield surface temperature is reached.

The program approach was to progressively narrow the choice of materials (alloys, coatings, insulation) and structural design of the columbium alloy TPS until a single, practical system could be selected and demonstrated in full-scale test. A three-phase work plan was followed.

Phase I (ref. 1) was initiated by selecting a model vehicle with an associated total environment from prelaunch to landing. This vehicle and environment formed the basis for the design conditions, design criteria, and test conditions used throughout the program. This selection was followed by an experimental and analytical evaluation of the



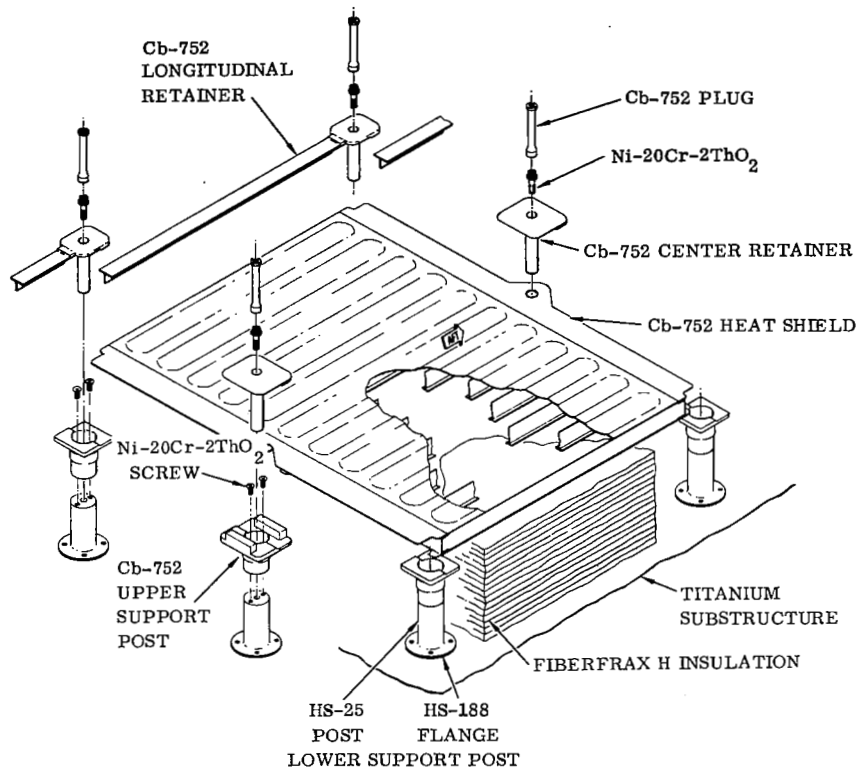


Figure 1. The Metallic TPS Concept

properties of available material systems. Phase I culminated in the selection of two material systems (Cb-752/R-512E and C-129Y/R-512E) for further evaluation.

Phase II (ref. 2) consisted of two parts involving two types of panels. Part 1 entailed the analytical investigation of seven heat shield structural configurations. The two most promising concepts were selected for subscale panel fabrication and testing using both materials. From these results, the better performing of the two material systems (Cb-752/R-512E) was selected for further evaluation. In Part 2, a complete TPS (i. e., heat shields, support structure, and insulation) was fabricated for each of the two configurations for testing under hot gas flow and radiant heat with applied loads at reduced pressures and supplemental acoustic testing. Also investigated were the forming, machining, and joining methods to be used for the fabrication of complete thermal protection systems. Based on the total performance of the two TPS configurations, one concept was selected for full-scale, full-size system evaluation.

In Phase III (ref. 3), a test specimen consisting of a full-scale, nine-panel array representative of an orbiter vehicle lower surface was fabricated. This specimen was exposed to simulated mission cycles of combined thermal and acoustic loads. Phase III demonstrated the structural and thermal adequacy and the practicality of full-sized, coated columbium alloy thermal protection systems. Data necessary to project the performance and cost of these systems for Space Shuttle vehicles was also documented.

## MODEL VEHICLE AND ENVIRONMENT

The focus vehicle selected for this investigation was a Rockwell International high cross-range orbiter launched on a Convair recoverable booster. Figure 2 illustrates predicted maximum surface temperatures for the selected orbiter. As shown, only the extreme nose tip and wing and tail leading edge temperatures exceed 1590 K (2400° F). A region of severe heating (see fig. 3) was selected as the area of investigation in all subsequent work. The maximum temperatures in this region vary from 1590 K (2400° F) at the forward edge to 1370 K (2000° F) at the aft edge. The environmental parameters were based on the most severe case, at the forward edge of the region.

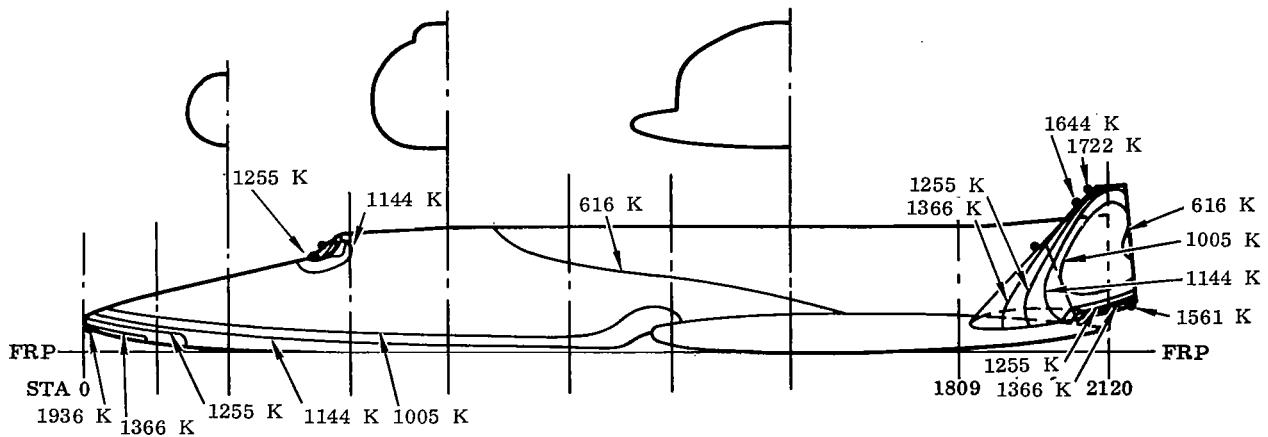


Figure 2. Predicted Orbiter Maximum Surface Temperatures

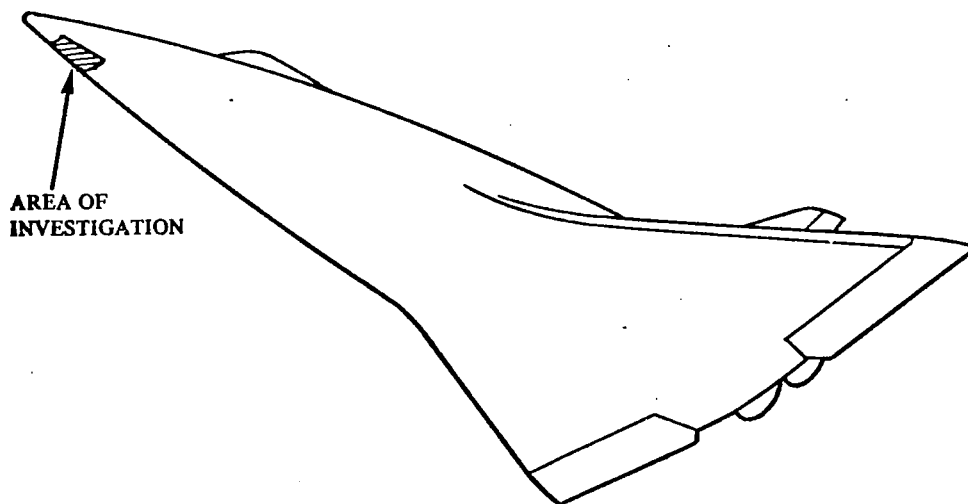


Figure 3. Selected Area of Investigation

The various flight conditions were combined into the design profile shown in figure 4. The critical loading occurred during launch at  $t=170$  seconds when the pressure differential load was  $20.7 \text{ kN/m}^2$  (3.0 psi) and the temperature was  $445 \text{ K}$  ( $340^\circ \text{F}$ ). As the temperature increased to  $790 \text{ K}$  ( $960^\circ \text{F}$ ) during staging, the pressure differential decreased to  $14.1 \text{ kN/m}^2$  (2.0 psi). During reentry the design load was step functioned from  $1.03 \text{ kN/m}^2$  (0.15 psi) during the maximum heat shield surface temperature of  $1590 \text{ K}$  ( $2400^\circ \text{F}$ ), to  $3.10 \text{ kN/m}^2$  (0.45 psi), and finally to  $5.86 \text{ kN/m}^2$  (0.85 psi) during the final stages of entry when a 2.5g maneuver would be performed. The maximum panel temperature after 2500 seconds of reentry would be below  $480 \text{ K}$  ( $400^\circ \text{F}$ ).

Using this thermal/structural profile, the main structural considerations were to design a TPS that (1) had minimum weight and volume, (2) was reusable for 100 missions, (3) was externally removable from the vehicle, (4) permitted inspection, and (5) accommodated thermally and mechanically induced stresses, deflections, and rotations.

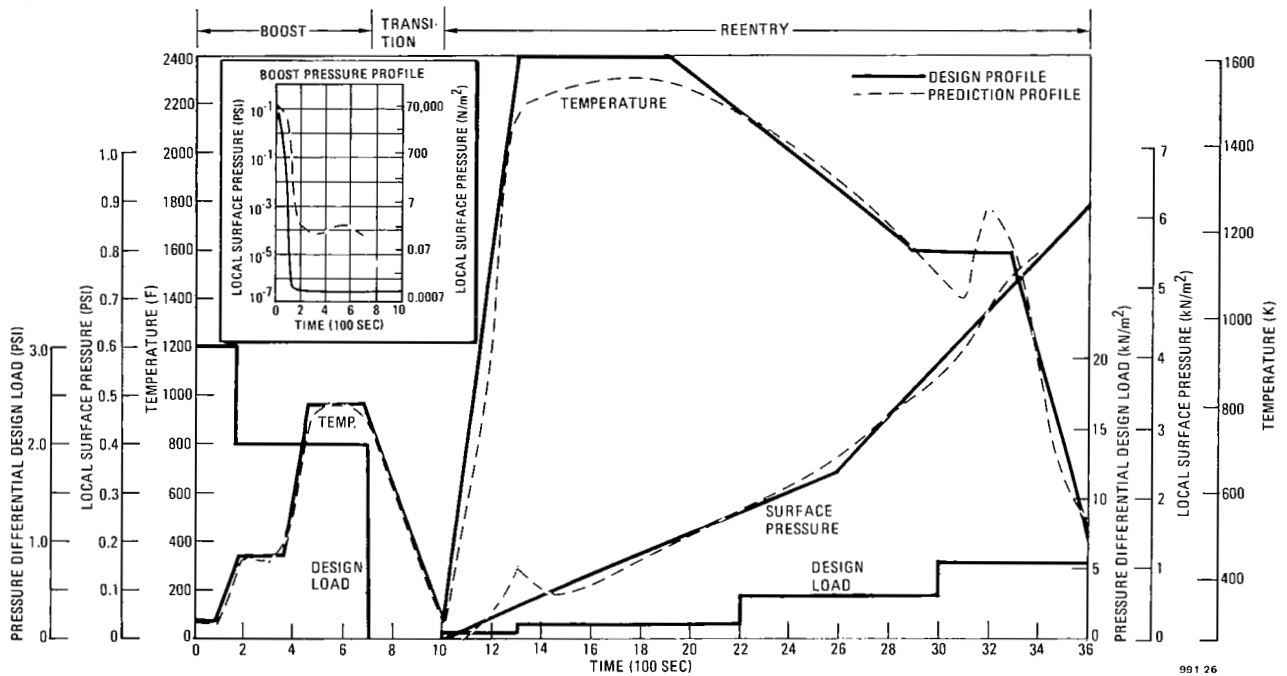


Figure 4. Design and Test Profile

### HEAT SHIELD CONFIGURATION STUDY

The efforts of this program were directed toward developing a metallic radiative TPS with maximum concern for structural reliability. Since columbium alloys require a coating to resist oxidation and therefore maintain structural integrity, fabrication methods with concern for coating application are extremely important. To assure adequate coverage of the components, the details must be fully inspectable by any one or

more of a variety of techniques. Similarly, the structure must be inspectable with reasonable ease between missions within a given turnaround time. Those components that are questionable for an additional mission must be easily removable for repair or replacement. All of these factors can increase the system weight. However, the weight of the system cannot be permitted to jeopardize the mission payload. With these factors apparent, a parametric study was undertaken to evaluate several candidate heat shield configurations.

The study exemplified the interaction of the various disciplines involved. An evaluation was made by applying weighting factors to particular parameters for each heat shield concept. Ranking and net worth of each of the five parameters shown in table I were determined by experienced personnel from each of the involved disciplines; i. e., design, structural analysis, weight analysis, fabrication and process development, cost analysis, and nondestructive evaluation.

TABLE I  
HEAT SHIELD CONFIGURATION  
EVALUATION

Parameter	Basis	Weighting Factor
Reliability	Usable for 100 flights	0.35
Weight	Pounds of system	0.25
Inspectability	(1) Time to initially inspect (2) Time to inspect within given turnaround	0.20
Fabrication	Time and material	0.10
Refurbishment	Time to replace or repair within given turnaround	0.10
		1.00

Preliminary designs of seven basic heat shield configurations, three methods of support, and two alloys were submitted for trade studies. The original concepts were: honeycomb sandwich, bead-stiffened, rib and tee-stiffened, grid-stiffened, vee-flat corrugation stiffened, and open corrugation. Tubular support posts, clips, and cantilevered channels were considered but not analyzed as an integral part of the preliminary study. A hinged panel concept was also proposed. This would have offered a system that was readily inspectable; however, assembly difficulties and corner gaps rendered this design impractical.

The trade study was based on heat shields of the general size 30.5 by 40.6 cm (12 by 16 inches) and the design profile shown in figure 4. In the structural analyses, the panels were considered to have simply supported edge conditions with joints that permit free thermal expansion. Five configurations had ribs or corrugations (in the direction of flow) that behave essentially as simply supported beams under normal pressure loading. The remaining two configurations were treated as plates. The short span, 30.5 cm (12 inches), minimum gages, and stiffener spacing, in general, dictated the section geometry. The analysis was composed of:

- (1) Ultimate static strength
- (2) Maximum creep strain
- (3) Maximum total deflection (pressure loading and permanent creep)

In addition each panel was designed to be unbuckled at limit load, since it is considered that local bending deformation associated with buckling would enhance cracks in the coating and possibly initiate failure. No change in material properties due to the effects of accumulative exposure to elevated temperature was made for the parametric study. However, the effective material thickness was assumed to be progressively reduced by 0.0025 mm (0.0001 inch) per side per flight. A linear rate of diffusion was assumed between the coating and substrate. To account for the effective thickness in the creep strain analysis, the design life of 100 missions was simulated in groups of 10 flights with the increment of creep strain and coating diffusion in each time interval factored by 10. Redistribution of internal stress due to accumulated creep strains was included in the analysis.

The critical design environments were established from the flight profile. Generally, the boost environment governed the structural sizing of the heat shield and its supports. Both buckling and static strength were critical at boost phase load levels. The heat shield panels were sized so that they sustained normal air loads and were of sufficient stiffness to resist panel flutter. The standoffs were sized so that they transmitted the panel air load to the main body structure, provided slip joints to accommodate thermal expansion, and minimized the number of thermal shorts.

Initially, the panels and their components were sized to withstand the boost pressure loads that occurred near maximum dynamic pressure and at low material temperatures. The panel size and gages were then checked for combined mechanical and thermal stresses at the maximum aerodynamic load condition and the maximum surface temperature condition. Finally, thermal distribution through the thermal protection and structural system was determined. In all cases, the panel size and the heat shield components were limited to a combined stress resulting from air loads, inertia loads, and thermal loads that were below the selected material allowable for crippling, compressive yield, and tensile yield. Once the size had been established, the heat shield was examined to determine that no combinations of load (including dynamic load) and temperature produced deflections or rotations that would cause permanent set or create hot spots.

Following the preliminary structural considerations, the heat shields were examined for fabricability and inspectability as shown in table II. Consideration was given to the number of elements and complexity of the parts required to make up a panel. Three methods of joining were considered: brazing, diffusion bonding, and welding. Since the panels were to be silicide coated, each concept was assessed for the ease of coating application and degree of inspectability.

The examination of manufacturing complexity considered tooling, number of parts, assembly procedures and sequence, number of available processing options, state-of-the-art or developmental needs, risk factors, and confidence levels.




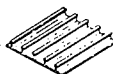



**TABLE II**  
**HEAT SHIELD CONCEPT SUMMARY**

TPS PANEL CONCEPT	ELEMENTS	Joining (▲ Indicates Preferred Process)									Coating		Mfg.	System
		Skin/Stiffener Joint ①			Beam-Doublers/Stiffener Joint ②			Beam-Doublers/Skin Joint ③			Application	Inspection	Complexity	Refurbishment
		Braze	Diff. Bond	Fusion Weld	Braze	Diff. Bond	Fusion Weld	Braze	Diff. Bond	Fusion Weld	(Rankings by Increasing Difficulty)			
<p>BEADED 12 IN. (TYP.) 16 IN. (TYP.) B TYP. 11 BEADS STIFFENER SKIN</p>	<p>1 SKIN 1 BEADED STIFFENER 2</p>	Δ	▲	—	← NONE (NO BEAM) →			← NONE (NO BEAM) →			7	5	1	3
<p>TEE STIFFENED STIFFENER DOUBLER CAP WEB SKIN</p>	<p>1 SKIN 12 RIBS &amp; CAPS 2 BEAM DBLR. 15 (MFG. WITH 2 SKINS)</p>	Δ	Δ	▲	Δ	—	▲	Δ	▲	—	4	4	4	2
<p>CORRUGATION STIFFENED STIFFENER DOUBLER SKIN</p>	<p>1 SKIN 1 STIFFENER 2 BEAM DBLR. 4</p>	Δ	▲	—	Δ	▲	—	Δ	▲	—	6	6	5	4
<p>HONEYCOMB SANDWICH SKIN CORE DOUBLER ALTERNATE DESIGN SEAL WELD</p>	<p>2 SKINS 1 CORE 4 BEAM DBLR. 7</p>	Δ	▲	—	Δ	▲	—	Δ	▲	—	1	1	7	5
<p>ISOGRID STIFFENED RIBBON DOUBLER FLATS SKIN</p>	<p>1 SKIN 14 RIBBONS 4 BEAM DBLR. 19</p>	Δ	▲	Δ	Δ	Δ	▲	Δ	▲	—	5	7	6	5
<p>OPEN CORRUGATION SKIN DOUBLER SKIN</p>	<p>1 SKIN 2 BEAM DBLR. 3</p>	← NONE (NO STIFFENER) →			← NONE (NO STIFFENER) →			Δ	▲	—	2	2	2	1
<p>RIB STIFFENED RIB DOUBLER SKIN</p>	<p>1 SKIN 12 RIBS 2 DOUBLERS 15</p>	Δ	Δ	▲	Δ	—	▲	Δ	▲	—	3	3	3	2

The coatability aspect considered the cleaning and ease of application for dipping, spraying, and edge overcoating. The ability to inspect the joints and coating is of sufficient importance as to impact the panel design; therefore, each configuration was evaluated for its ability or complexity to be inspected by visual means as well as by radiography, electron-emission, thermoelectric emission, and ultrasonics.

Each configuration was graded for structural performance, reliability, weight, ease of fabrication, refurbishability, and inspectability. Ultimately each configuration was evaluated on the basis of an idealized structure having a value of 10. An idealized columbium alloy configuration was assumed that would best satisfy the following criteria: allow all surfaces to be coated, minimize faying surfaces before coating, maximize edge and corner radii and minimize coating strains, be fully inspectable, minimize use of coated fasteners, minimize sliding load-carrying surfaces, avoid contact with incompatible materials, and have minimum weight and cost (ref. 4). Every effort was made to make the study objective. Hence, a method was used for applying weighting factors that indicated the relative importance of each parameter. Factored ratings were then totalled as shown in table III.

TABLE III  
COLUMBIUM ALLOY HEAT SHIELD CONFIGURATION SELECTION

Concept	Reliability (0.35)		Weight (0.25)		Inspectability (0.20)		Fabricability (0.10)		Refurbishability (0.10)		Weighting Factor Total	Overall Ranking
	5	1.75	5	1.25	9	1.80	3	0.30	5	0.50		
	5	1.75	5	1.25	9	1.80	3	0.30	5	0.50	5.60	4
	5	1.75	6	1.50	5	1.00	6	0.60	3	0.30	5.15	5
	6	2.10	6	1.50	7	1.40	6	0.60	6	0.60	6.20	3
	6	2.10	8	2.00	6	1.20	5	0.50	6	0.60	6.40	2
	3	1.05	7	1.75	5	1.00	5	0.50	5	0.50	4.80	7
	4	1.40	6	1.50	5	1.00	7	0.70	4	0.40	5.00	6
	8	2.80	9	2.25	9	1.80	9	0.90	9	0.90	8.65	1

↑ ↑ Factored Rating

Concept rated on basis of 10

Based on the five parameters considered, the results of this trade study indicated that the two most favorable concepts were the open corrugation and the tee-stiffened heat shields as evidenced in table III. Subsequently, these configurations were fabricated into subsized panels to evaluate the degree of coatability for each of two alloys in configuration form, and then into complete, small-size TPS specimens for further evaluation.

## TPS DESIGN

In addition to maintaining structural integrity with the minimum thermal mass, one of the principal design objectives was to minimize the quantity of mechanical fasteners in general and to eliminate refractory metal fasteners in locations where their removal would be necessary for TPS inspection and repair. Also, it was desirable to have a minimal but controlled surface leakage. A considerable variety of "optimum" heat shield sizes was open to the designer, the largest size restriction 61 by 91 cm (24 by 36 inches) being imposed by the working zones of available heat treating and coating fusion furnaces. The configuration size directly imposed was that of test facilities. A heat shield size of 30.5 by 40.6 cm (12 by 16 inches) was selected, which provided for a region of unaffected edges in a thermal test area of approximately 56 by 56 cm (22 by 22 inches) for the small-size TPS series. This heat shield size was also employed for the proof-of-concept, nine-panel array in order to use common tooling.

An exploded assembly view of the tee-stiffened TPS used in the nine-panel array was shown in figure 1. The panel is designed to react positive and negative pressure loadings to the supporting primary structure by two integral transverse beams. The heat shields are shingled in the forward and aft directions and are free to thermally expand about a fixed location near the center of the trailing edge. The heat shield is supported by split tubular support posts — the upper portion being Cb-752 and the lower section being a dispersion strengthened metal or superalloy. The bi-metal posts were designed such that a transition from Cb-752 to the superalloy was made at a region where the predicted temperatures were near 1370 K (2000° F).

In addition to taking advantage of the lower thermal conductivity [a factor of 2 at 1370 K (2000° F)] of the superalloy, it also permitted the use of fasteners that were considerably less troublesome than coated refractory metal fasteners. Finally, the panels are restrained from vertical and translational motion at the center of the transverse edges by a capped post and along the longitudinal edges by a tee-beam with an integral post. These posts are inserted through the upper Cb-752 support post and attached with an Ni-20Cr-2ThO<sub>2</sub> bolt. A Cb-752 plug is inserted into each of the six posts and threaded onto the Ni-20Cr-2ThO<sub>2</sub> bolt. All of the Ni-20Cr-2ThO<sub>2</sub> components were coated with an aluminide to minimize any potential reaction with the silicide coating of the Cb-752. The system is insulated with ceramic fiber blanket insulation.



The thermo/structural analysis of the panels was greatly simplified by the design itself in that provisions for free expansion of the panel, eliminating extreme thermal stresses, were provided. The critical thermal stresses, as a result of this expansion capability, do not occur at maximum heat shield temperature but at lower temperature at a time when the temperature gradients are highest. Two boost phase conditions covering maximum crushing  $21 \text{ kN/m}^2$  (3 psi) with modest temperature gradient  $345 \text{ K}$  ( $159^\circ \text{F}$ ) and maximum burst  $14 \text{ kN/m}^2$  (2 psi) pressure with similar temperatures were checked. One entry condition with the maximum temperature gradient of  $395 \text{ K}$  ( $252^\circ \text{F}$ ) but low pressure  $4.2 \text{ kN/m}^2$  (0.15 psi) was also checked.

The mechanical loads and stresses were considered using a simple beam analysis, which is quite accurate for the determinate panel support arrangement. The thermal stresses were analyzed separately (using a numerical analysis similar to a finite element technique) and then summed with the mechanical loads. The procedure is fairly simple, but it yields a detailed stress picture. All margins were positive, with the critical margins for skin buckling under crush loads at ultimate pressure. A fatigue and acoustic analysis was also run and indicated high margins of safety, also.

The second concept evaluated in Phase II was the open-corrugation TPS. It is shown in figure 5 in an exploded assembly view. Again, the heat shields are shingled fore and aft.

The panel employs transverse beams for stability with transverse panel expansion being accommodated by the corrugation deflection. Except for the aft center panel support post that is bolted permanently to the transverse beam, the tubular support posts and access are as previously described. However, note the material differences of the lower support posts and the insulation. These changes were made between Phase II when the open-corrugation TPS was conceptually evaluated and Phase III when the final tee-stiffened TPS configuration shown in figure 1 was selected.

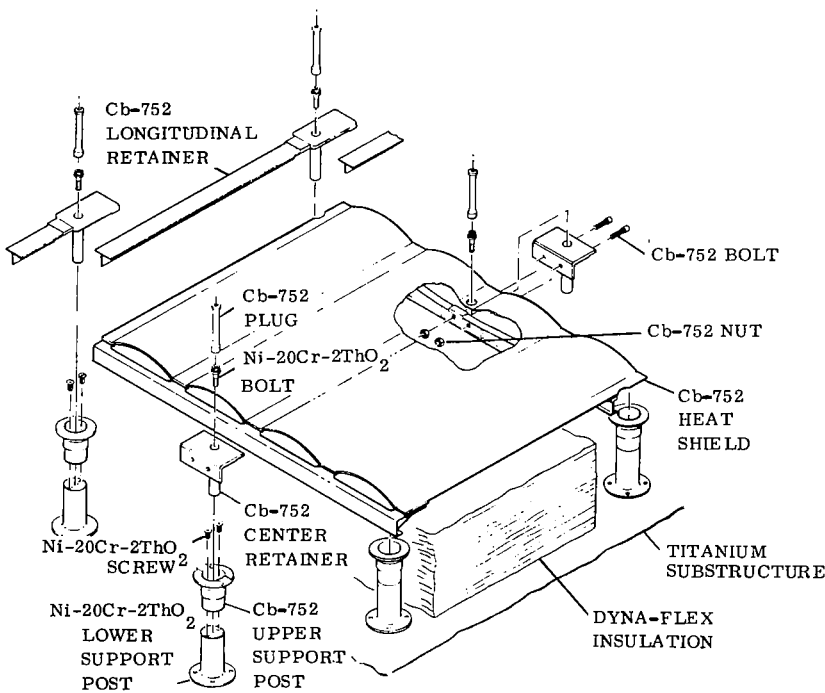


Figure 5. Open-Corrugated TPS Exploded Assembly

## ELEMENTAL SPECIMEN TESTING

Flight simulation testing was the primary part of an experimental investigation of material system characteristics for heat shield applications. Two columbium alloys Cb-752 (Cb-10W-2.5Zr) and C-129Y (Cb-10Hf-10W-0.1Y) each with two silicide coatings R-512E (Si-20Cr-20 Fe) and VH-109 (duplex Si-Hf-Ta-Cr-Fe) were evaluated for four types of specimens (parent metal, electron beam welded, diffusion bonded, and brazed). In addition alloy WC-3015 was to be evaluated. However, this material was available in limited quantities and sheet sizes. WC-3015 was found to be highly weldable but some sheet delamination was present in the material received. In addition, annealing and coating operations resulted in very low room temperature ductility. Because of the low ductility, WC-3015 was eliminated from the flight simulation test program.

The elemental test profile used for the flight simulation testing closely followed the predicted boost and entry trajectory histories. The total test time per cycle was 3600 seconds. All essential parameters could be performed within this time period, and it was consistent with equipment operating time. A ramp function temperature profile was selected to more easily analyze and correlate test results. The peak temperature during the simulated boost phase was 790 K (960 °F), which was maintained for 200 seconds before returning to room temperature. The simulated entry temperature profile exhibited a peak temperature of 1590 K (2400 °F) in 300 seconds and was held for 600 seconds. The temperature was decreased in 1000 seconds to 1145 K (1600 °F) and was held for 400 seconds before returning to room temperature.

The test load profile represented the load due to pressure differentials associated with the flight. That is, up to 21 kN/m<sup>2</sup> (3 psi) might be experienced during the booster launch phase (t=0 to 170 seconds) when the booster/orbiter interference effects might be present. This load creates a nominal skin bending stress level of 200 MN/m<sup>2</sup> (29 ksi). Up to 14 kN/m<sup>2</sup> (2 psi) might be experienced later in the launch phase, creating a skin bending stress level of 130 MN/m<sup>2</sup> (19 ksi). The pressure differentials vary with entry and were raised slightly during the last step to account for maneuvers expected during the cruise phase. The nominal bending stress levels ranged from 10.3 MN/m<sup>2</sup> (1.5 ksi) at maximum temperature [1590 K (2400 °F)] to 28 MN/m<sup>2</sup> (4 ksi) and to 55 MN/m<sup>2</sup> (8 ksi) during the latter stages of the profile.

A total of 80 specimens was exposure tested in the flight simulation portion of the test program. The results are summarized in table IV. These specimens received 7124 total cycles with 47 completing 100 cycles and 33 failing in from 42 to 97 cycles. The term "failure" as used for these tests denotes complete specimen fracture.

Results of the flight simulation exposures indicate the superiority of the HiTemCo R-512E coating over the Vac-Hyd VH-109 coating. Of the 44 R-512E coated specimens, 43 survived 100 cycles, which gives a survivability mean of 99.9 cycles. No differences

TABLE IV

## FLIGHT SIMULATION TEST RESULTS FOR ELEMENTAL SPECIMENS

Alloy	Coating	Condition	Cycles						Mean
Cb-752	R-512E	Parent	100	100	100	100	100	100	99.8
Cb-752	R-512E	EB Weld	100	100	100	100	100	97*	
Cb-752	R-512E	Diff Bond	100	100	100	100	100	100	
Cb-752	R-512E	Braze (0.08 overlap)	100	100	100	100			
Cb-752	R-512E	Braze (0.30 overlap)	100	100	100	100			
Cb-752	VH-109	Parent	89*	85*	84*	83*	69*	42*	64.3
Cb-752	VH-109	EB Weld	65*	61*	61*	57*	50*	49*	
Cb-752	VH-109	Diff Bond	75*	69*	61*	58*	55*	44*	
C-129Y	R-512E	Parent	100	100	100	100	100	100	100
C-129Y	R-512E	EB Weld	100	100	100	100	100	100	
C-129Y	R-512E	Diff Bond	100	100	100	100	100	100	
C-129Y	VH-109	Parent	100	100	100	91*	86*	78*	87.2
C-129Y	VH-109	EB Weld	100	94*	90*	89*	79*	62*	
C-129Y	VH-109	Diff Bond	96*	89*	88*	80*	74*	74*	

Note:\*Indicates failure

80 specimens

7124 total cycles

were observed in the performance of the parent metal specimens and the joint evaluation specimens. Only 4 of the 36 VH-109 coated specimens completed 100 cycles. The VH-109 material system resulted in a survivability mean of 75.8 cycles. The Cb-752/R-512E specimens exhibited a mean cyclic creep of 2.33% for 100 simulated missions. The C-129Y/R-512E specimens exhibited a mean cyclic creep of 2.01% for 100 simulated missions. Predicted cyclic creep strains in both cases were approximately 1%.

Twelve tensile specimens representing samples of the four candidate alloy/coating systems were also tested by plasma arc heating. The purpose of these tests was to evaluate the effect of high velocity ( $m=3.3$ ), high temperature air on the materials, as opposed to the still air radiant heating tests previously described. The tests simulated the entry portion of the heating profile shown in figure 4, with an oxygen-nitrogen mixture as the test stream. The specimens were mechanically loaded during test to the expected design tensile stress.

The experimental set-up proved difficult and many of the specimens failed prematurely as the result of local overheating from secondary shock wave impingement. Shock impingement occurred on the leading edge of the specimens, causing fairly rapid damage and breakdown of the coating. A buffer "dummy" specimen was used as a shield in the test series, but was not adequate to prevent secondary impingement on the edge of the other specimens. The specimens were tested in groups of four. The first group was used to progressively modify the test series in terms of feedback control and plasma parameters and produced no meaningful material data.

Of the remaining specimens, three survived 40 mission cycles of the entry heating profile without edge erosion, and the other five had indications of moderate to severe edge erosion. The tests led to the following conclusions:

- (1) Failures initiated only when flow discontinuities occurred in the vicinity of the specimen edge, a condition which can be eliminated by careful TPS design.
- (2) Damage sites did not result in catastrophic failure of the substrate. The loaded specimens sustained more than one simulated entry cycle after initial coating breakdown.
- (3) There is a decided difference between the performance of a damage site under static conditions and high mass flow air environments. The rate of edge erosion during static air simulation tests was 0.0064 cm (0.0025 in.) per mission cycle. The rate of edge erosion during the plasma arc tests was between 0.13 and 0.54 mm (0.005 and 0.021 in.) per cycle.

Based on the visual observations of coating behavior during cyclic flight simulation testing as described in this section, the four material systems were rated in the following order: Cb-752/R-512E, C-129Y/R-512E, C-129Y/VH-109, and Cb-752/VH-109. Therefore, the R-512E coating was selected to be applied to subsized heat shield configurations fabricated from each of the two alloys.

#### RESIDUAL MECHANICAL PROPERTIES

The tensile properties for Cb-752/R-512E generated under this program were initially evaluated on the basis of uncoated cross-sectional areas. These values have been adjusted on the basis of the estimated area remaining after coating and after cycling where applicable. The calculations conservatively assume a nonstructural diffusion zone. For the application of 0.076 mm (3 mils) of coating per side, it was assumed that 0.25 mm (1 mil) of base metal was consumed. It was experimentally determined in ref. 1 that an average of 0.0127 mm (0.0005 inch) of substrate was consumed for the 100-cycle exposure. Plots of the adjusted test data after 100 cycles for ultimate strength and tensile yield versus temperature are presented in figures 6 and 7 (ref. 5 and 6). Preliminary design curves (used for the small-size test specimens) and recommended design curves are also given. The recommended design curves generally follow the "A" values of reference 6 except where data points from other sources fall below the reference 6 curve. The curves are presented as conservative approximations only since, in general, axial tension properties were not critical for design.

Creep data spanning the time period and elevated temperature range expected during Space Shuttle orbiter reentry performance were required for design evaluation of the coated columbium alloy TPS. Data presented herein are for the most promising material system (Cb-752/R-512E) at temperatures from 1370 K (2000° F) to 1590 K (2400° F).

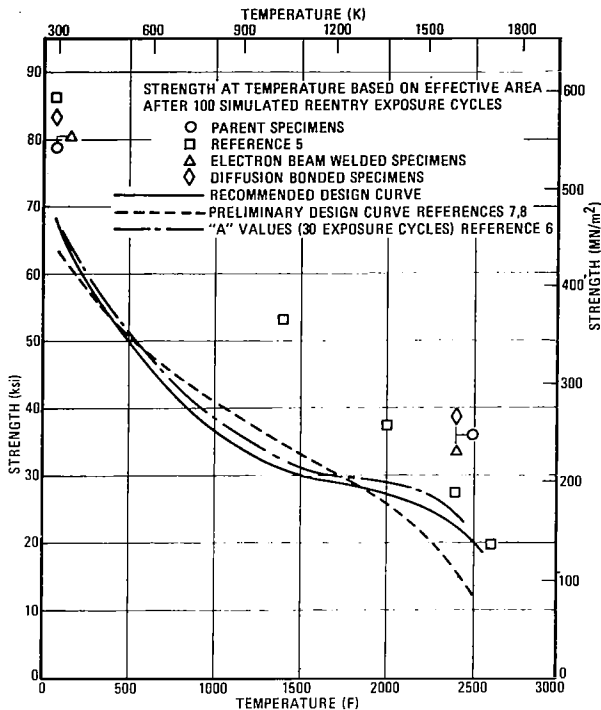


Figure 6. Ultimate Strength of Cb-752/R-512E After 100 Cycles

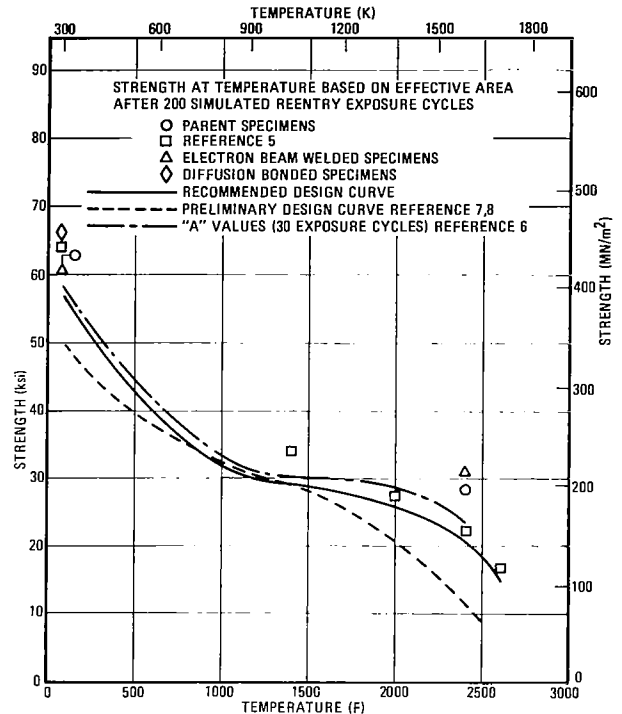


Figure 7. Yield Strength of Cb-752/R-512E After 100 Cycles

The target was to provide stress levels covering the range of 10 to 100 hours for 1% creep. The stress levels were calculated on the basis of the original metal thickness prior to coating. Composite creep curves for 0.5%, 1%, and 2% creep are presented in figure 8.

### MICROMETEOROID IMPACT TESTS

It is required that the Space Shuttle orbiter be designed to tolerate prolonged exposure to the micrometeoroid environment without undue hazard to the crew and without excessive maintenance of the exposed surfaces. Preliminary meteoroid hazard analysis indicated that thermal protection systems based on the use of thin heat-resistant materials will sustain erosion, cratering, and a few punctures of the outer surface, which could be incompatible with this requirement.

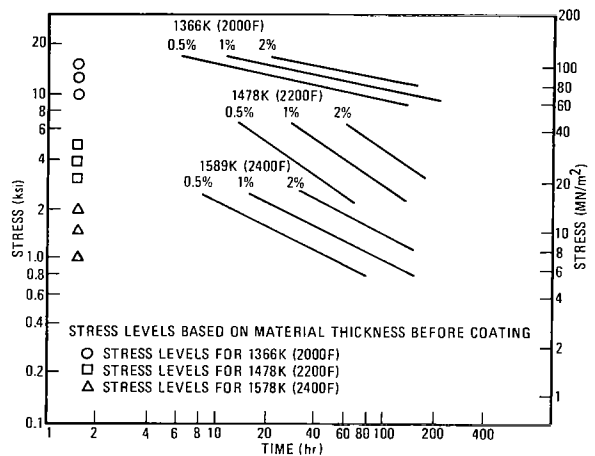


Figure 8. Creep Properties of Cb-752/R-512E at 1370 K (2000° F), 1480 K (2200° F) and 1590 K (2400° F)

The testing of coated columbium alloy specimens under this program was intended to provide data for representative heat shield gages. The tests and data would then be related to post-impact thermal exposure, repair techniques, and verification of penetration mechanics.

Two types of specimens were provided for testing: (1) 5.08 by 5.08 by 0.051 cm (2 by 2 by 0.020 inch) coupons, and (2) standard 0.038 cm (0.015 inch) thick tensile specimens from Phase I of the program. All specimens were coated. Two types of the square coupons were impacted – eight as-coated/unexposed and eight that were subjected to 50 simulated flight cycles to 1590 K (2400°F). Of the six tensile specimens two had sustained 50 Phase I flight simulation cycles and four were as-coated. These four specimens were exposed to 50 flight simulation cycles after bombardment.

### Erosion Tests

Erosion testing was performed in a Vandergraph facility at Langley Research Center. Six tensile specimens were supplied as part of the Phase I flight simulation test program. Each specimen was impacted with 700 particles/cm<sup>2</sup> with a particle mass of  $2.62 \times 10^{-10}$  grams at an average velocity of 14 km/sec.

Four of the specimens had been previously exposed to 50 flight simulation cycles and two had no previous exposure. After bombardment all specimens were visually examined. Using magnifications up to 250X no difference could be detected between the material surface in the impact zone and that of the surrounding region. This indicated that the microparticles had caused negligible damage. Two of the specimens were metallographically examined but no effect of the bombardment was revealed.

The remaining specimens were subjected to 50 flight simulation cycles. No unusual surface conditions were observed following this exposure. These specimens were subsequently tensile tested with the results indicating no significant material property changes.

### Cratering Tests

Eight specimens were provided for the cratering tests – six C-129Y/R-512E and two Cb-752/R-512E. Prior to bombardment, four of these specimens were subjected to 50 slow reduced pressure cycles to 1590 K (2400°F).

The test projectiles were 0.005 cm (0.002 inch) diameter glass spheres having a density of 2.3g/cm<sup>3</sup> and a mass of  $1.57 \times 10^{-7}$  gram. The particle velocities ranged from 5 to 15 km/sec. The particles were energetic enough to cause visible craters in the surface of the specimens but not powerful enough to cause perforation.

Following bombardment and electron emission radiographic mapping all specimens were subjected to 50 slow reduced pressure cycles to 1590 K (2400° F). These specimens exhibited no unusual surface oxidation and no substrate erosion.

### Perforation Tests

Eight specimens were also provided for the perforation tests – six Cb-752/R-512E and two C-129Y/R-512E. Two Cb-752/R-512E and two C-129Y/R-512E were thermally exposed while four Cb-752/R-512E were unexposed.

The perforation tests were performed in a light gas gun facility. The test projectiles were 0.081 cm (0.032 inch) aluminum spheres having a density of 2.78 g/cm<sup>3</sup> and a mass of  $7.74 \times 10^{-4}$  gram. The particle velocities ranged from approximately 3 to 7 km/sec. A 2024-T3 aluminum plate was located 2.54 cm (1 inch) behind the coupon to obtain data on the debris cloud particles. A group of the specimens following bombardment and prior to subsequent thermal exposure is shown in figure 9.

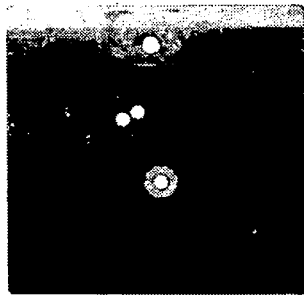
The 2024-T3 aluminum rear sheets located behind the columbium alloy specimens were pitted over a 3.81 cm (1.5 inch) diameter area by impact of projectile and target fragments. Using an optical microscope the deepest pits were found to be located near the center of the damage circle. Theoretical penetrations, as determined by the computer program of reference 7, were correlated with these values, and it was found that predicted penetrations were low by an average of 4%. As this is probably less than the experimental scatter, it was concluded that these test results support the usage of the subject program for damage predictions on the two types of coupons tested.

Following bombardment, the four specimens shown in figure 9 were examined, repaired, and thermally cycled. In figure 9 it can be noted that in addition to the through-penetrations, the specimens also exhibit secondary damage sites. Specimens 1, 2, and 3 are shown in the as-bombarded condition with no thermal exposure. Specimen 5 sustained 50 thermal cycles prior to being bombarded.

If a vehicle was bombarded by micrometeoroids and sustained detectable damage while on station, the options are: (1) to replace the damaged heat shield (by ferrying a replacement part to the vehicle or by an on-board store), (2) repair the damaged areas (this is feasible, especially by using the plug repair method, ref. 8), or (3) reenter the atmosphere without repair. The first two options present little or no problems for reentry. However, the question is posed whether or not a vehicle could safely reenter with damaged columbium alloy heat shields. (The problem of subsequent insulation damage or thermal effects of hot air ingestion would have to be evaluated.)

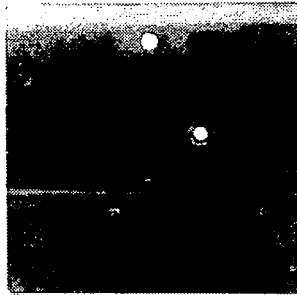
Using the penetration test data, where the projectile velocities ranged from approximately 3 to 7 km/sec, the resulting through-holes varied from 0.135 cm (0.053 inch) to

NO THERMAL EXPOSURE/BOMBARDED



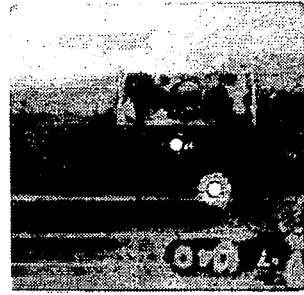
1

Cb-752/R-512E



2

Cb-752/R-512E



3

Cb-752/R-512E

THERMAL EXPOSURE/BOMBARDED



5

Cb-752/R-512E



Figure 9. Columbian Alloy Coupons after Bombardment and Thermal Exposure

0.201 cm (0.079 inch) diameter for the specimens previously exposed to 50 thermal cycles. For the unexposed specimens, the hole size ranged from 0.201 cm (0.079 inch) to 0.236 cm (0.093 inch) diameter, with the hole size being velocity dependent in all cases. Referring to the defect tolerance work at Battelle Columbus Laboratories (ref. 9), it was shown that under dynamic flow conditions an initial through-defect in Cb-752/R-512E and C-129Y/R-512E could increase in diameter from 0.102 cm (0.040 inch) to 0.254-0.356 cm (0.100-0.140 inch) after one cycle. [This increase of 2.5 to 3.5 times is related to temperatures ranging from 1630 to 1650 K (2470 to 2510° F).] Using this relationship the size of the aforementioned holes could increase as shown below.



Specimen Condition	Original Hole Diameter*		Projected Hole Diameter After 1 Reentry Cycle	
	cm	(in.)	cm	(in.)
50 thermal cycles	0.135	(0.053)	0.338-0.472	(0.133-0.186)
	0.201	(0.079)	0.503-0.704	(0.198-0.277)
No thermal cycles	0.201	(0.079)	0.503-0.704	(0.198-0.277)
	0.236	(0.093)	0.592-0.828	(0.233-0.326)

\*Hole sizes were velocity dependent

Since field repairs of columbium alloys have been made on defects up to 1.27 cm (0.50 inch) diameter (ref. 8), it is not unreasonable to assume that holes of the projected size could be repaired successfully and the heat shield reused.

Three of the four coupons shown in figure 9 were repaired. Specimen 3 (the unrepaired specimen) was subsequently exposed to slow cyclic temperature to 1590 K (2400° F) at reduced pressures in the as-defected condition. The base metal oxide was visible at the first inspection after six cycles. Testing was continued to 13 cycles, after which time the 0.201 cm (0.079 inch) diameter holes had grown to 0.66 cm (0.26 inch) diameter. No evidence of base metal oxidation was noted at secondary damage sites.

Specimen 2 was repaired with a plug using a high intensity spot heater. The 0.235 cm (0.093 inch) diameter hole was drilled out to 0.43 cm (0.17 inch) and a pure columbium plug was inserted. The specimen was repaired in five places on one side and four places on the other side to cover primary and secondary damage sites. After 20 cycles, base metal oxide was observed at an edge at the location of an accidental coating chip. Testing was continued to 50 cycles with no evidence of base metal oxide at any of the repair sites.

Specimens 1 and 5 were repaired using the glass repair method (ref. 8). Since these specimens exhibited the most primary and secondary damage, it was thought that the glass repair would give the best coverage and protection. Most of the sites were well covered. After 20 cycles a hole developed through the specimen at one of the repair sites. No evidence of base metal oxide was observed at 50 cycles nor did the hole enlarge significantly. Specimen 5 developed base metal oxide and a through hole after 20 cycles. This appeared to be at the site of an improperly repaired defect. Two additional sites of base metal oxide were observed after 38 cycles in unrepaired areas.

With the specimens employed it is apparent that good field repairs can be made and that heat shield sustaining severe damage (such as through-penetrations) can be made serviceable for many additional cycles. In observing the effects of the two repair processes there was no preference of one over the other. It appears that for relatively

large holes the heat lamp and plug method offers the surest repair. However, the process does concentrate heat over a rather small area and could cause localized panel distortion. The amount of distortion probably would be aerodynamically acceptable. The glass repair method appears to be simpler and affords excellent coverage and protection for a wide variety of damage sites.

## LIGHTNING STRIKE TESTS

The effect of lightning strikes on coated columbium alloy heat shields had not been defined prior to the initiation of this program. However, it was anticipated that problems with electrical bonding and intrastructural arcing could be aggravated by the presence of the non-conductive silicide coating. Also, it was theorized that charges induced by climatic electrical fields could build to a large potential at the coating surface and eventually break down the dielectric protection at attachments and edges of the heat shields. The resulting arcing could interfere with the operation of electrical systems or cause damage to the coating and expose the substrate to oxidation. Hence, two simulated heat shields were fabricated and tests established to investigate the phenomena of lightning discharge.

Two sets of specimens were fabricated from Cb-752. The heat shield was unstiffened and of the dimensions 26.7 by 26.7 by 0.038 cm (10.5 by 10.5 by 0.015 inches). The overall specimen size was 38.1 by 38.1 by 5.08 cm (15 by 15 by 2 inches). All components were coated with 0.076 mm (0.003 inch) thick R-512E. The heat shields were examined by electron emission radiography and thermoelectric probe and found to have a uniform coating. Prior to performing electrical resistance mapping measurements, one specimen was oxidized at 1590 K (2400°F) at one atmosphere for one hour in air. The second specimen was mapped in the unexposed condition thereby giving a relative comparison of electrical resistance between a first flight panel and one that had been thermally exposed. The resistance of the oxidized panel was found to be significantly greater than that of the unexposed panel.

To reproduce the various lightning strike effects on a columbium alloy heat shield three types of tests were conducted. The first was a high current rise discharge (maximum  $dI/dt$ ) of 100 000 amperes per microsecond fired into the specimen as specified in MIL-B-5087B. The high rate of rise is intended to produce induced surges in wiring, but also is an assessment of the ability of a material to dissipate (conduct) a charge away from a localized area without burning or damage. The results of this test on each skin was very slight pitting but no visible perforation to the substrate.

The second test was a maximum energy (maximum Q) test that is typical of a cloud-to-cloud, cloud-to-vehicle, or the second component of a cloud-to-ground discharge during which relatively low currents (less than 10 000 amperes) and long dwells

(milliseconds rather than microseconds) occur. Typically, this results in burned holes 0.64 to 1.91 cm (0.25 to 0.75 inch) diameter at wing trailing edges of an aircraft as charges accumulate and try to leave the wing. When brass electrodes were used, the results were slight pitting of the surface of each skin. However, during the arcing, the brass electrode was bombarded by columbium ions. Thus, brass sputtered from the electrode and onto the strike area of the panels. Since the presence of brass could cause premature coating failure or eutectic alloying with the columbium during subsequent thermal exposure, it was decided to use a tungsten electrode in the remaining test.

Thus, the test was repeated with a tungsten electrode and in the initial test the electrode apparently produced puncture of the skin through mechanical force. To produce a more realistic test in view of these two non-inflight effects, an intermediate discharge was triggered to the panels using a high voltage, low current trigger generator to establish an arc of 7.62 cm (3 inches) in length down to the test panel.

The results of the test showed very minor pitting on both samples and rather extensive spreading of the discharge contact points over an area of several square inches. Thus both panels passed the intermediate current, intermediate duration discharge tests with only minor pitting but some damage to the coating on the skin.

The third type of test was a high current discharge of 200 000 amperes. This would be typical of a major cloud-to-ground lightning strike and would normally puncture the aluminum skin of an aircraft. The hole would largely be the result of a mechanical shock wave. This is a ground, rather than flight, condition.

For both specimens, the discharges tore the simulated heat shield resulting in a fairly large hole in the columbium. It should be noted however that a 200 000 ampere return stroke would be expected to strike an extremity and not a mid-chord area, which is generally contacted by restrikes or continuing components. This current with a 20 000 ampere crest and a time duration of nearly 40 microseconds represented the initial high current component of a natural lightning discharge.

As an example the test specimen without prior thermal exposure is shown in figure 10. After electrical testing, each specimen was exposed to two 1/2-hour cycles to 1590 K (2400° F) in air to determine the oxidation resistance of the struck areas. As expected, the ruptured areas developed a heavy columbium oxide and the arc burns developed a light oxide. The arc burns could easily have been repaired but the test results indicate that, had a strike of this nature occurred during flight, the mission and recovery would not have been jeopardized.

In summary, the panels could withstand the maximum current use rate ( $dI/dt$ ) and a typical cloud-to-cloud discharge (high Q) without perforation. Some coating damage is possible within approximately a 1.27 cm (0.5 inch) radius. However, it is expected that at least one successful reentry could be made.

The maximum current strike, typical of a cloud-to-ground bolt, ruptured the panels causing the material to rip. Rips of approximately 2.50 to 5.25 inches (6.35 to 13.34 cm) along with inward bending of the ripped areas occurred. A panel damaged in such a manner would be unsatisfactory for reentry due to ingestion of the air stream. It would therefore, require repair or replacement prior to atmospheric entry. However, since the strike condition was an example of an on-the-pad mode, it is unlikely that the vehicle would be launched with a noticeably damaged heat shield.

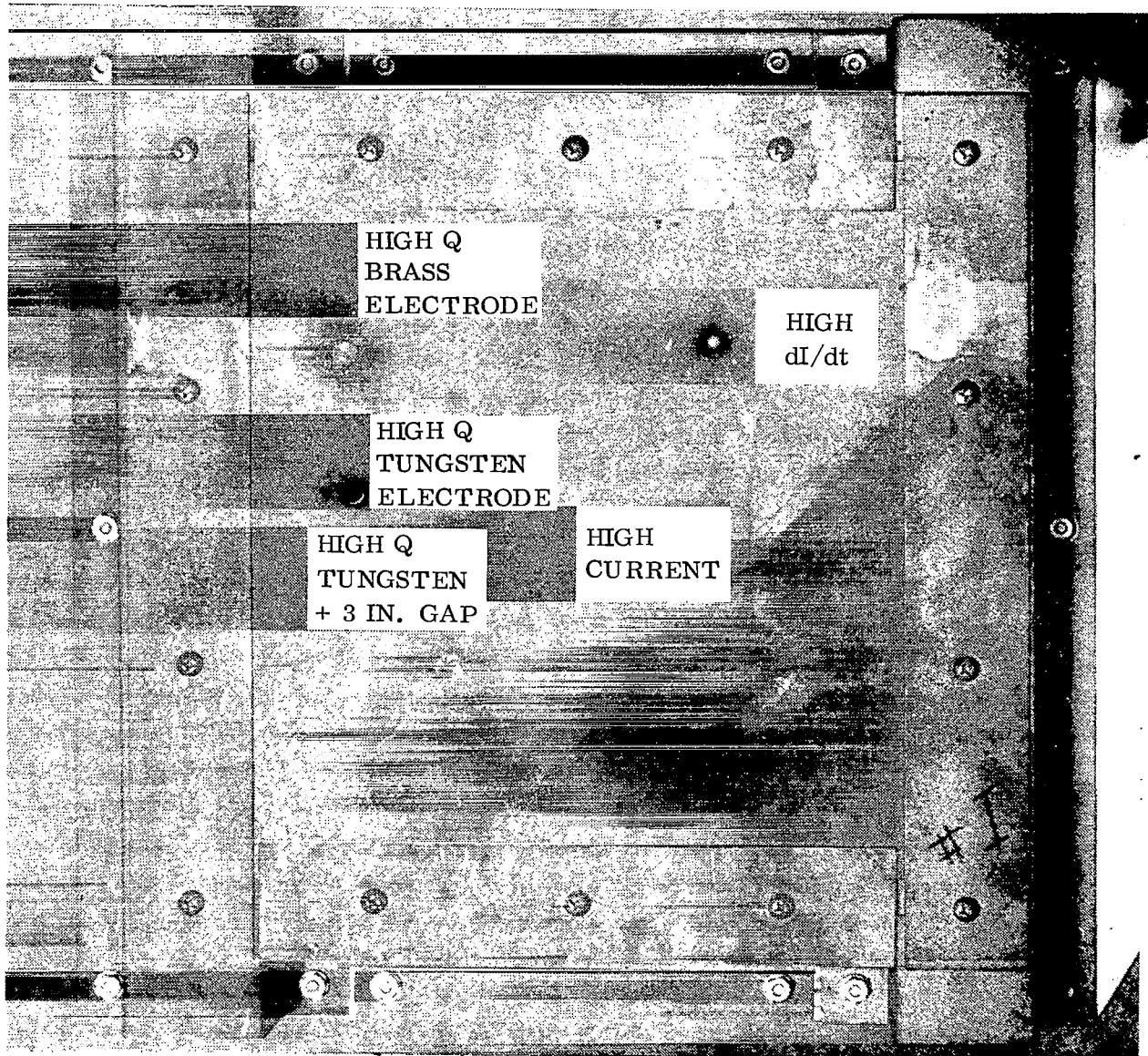


Figure 10. As-Coated Cb-752 Test Specimen After Lightning Strike Test Sequence

## SUBSIZE TPS PANELS

Following the material characterization study, structural configurations were evaluated. The two heat shield concepts (an open corrugation and a tee-stiffened) selected from the configuration trade study were fabricated from both Cb-752 and C-129Y alloys and coated with R-512E.

### Panel Fabrication

Each specimen type was designed to be tested in a chamber similar to but larger than that used for the elemental tensile specimens of the first phase of the program. The panels were 12.07 cm (4.75 inches) wide and 19.23 cm (7.57 inches) long. The corrugated specimens were 1.27 cm (0.50 inch) deep and the tee-stiffened specimens were 1.78 cm (0.70 inch) deep.

A corrugated panel (fig. 11) consisted of a single formed corrugation. Two straps bolted across the lower surface of the specimen at each end and one at the center. These straps, not shown in figure 11, served to offer constraint during testing in a manner similar to that afforded by adjacent corrugations in a full-size panel. The material thickness for the panel was 0.064 cm (0.025 inch) prior to coating.

A tee-stiffened panel shown in figure 12 consisted of a full face sheet or panel skin and three tee-shaped ribs. Each end of the panel had an angle-shaped load member that distributed the input loads into all of the ribs and the skin during testing and also served to stabilize the ribs. These angle members were welded to the panel skin and to the rib ends and were continuous extensions of the rib caps or flanges. All material used in the fabrication of these tee-stiffened panels was a nominal 0.020 inch (0.051 cm) thick prior to coating.

The fabrication sequence for a corrugated panel and that of a tee-stiffened panel are shown in figure 13. Both Cb-752 and C-129Y used in the fabrication of the panels possess nearly equal fabricability. Likewise, both alloys were considered to be equally as coatable with R-512E silicide coating and required identical preparation for coating.

The fabrication of the corrugated panel was quite simple and involved only a few normal sheet metal practices and processes. The only exception was the edge and corner preparation operation, which involved a rounding or radiusing of the surfaces manually, by vibrating finishing, or by a combination of both. This prepared the edges and corners with the best condition for the application of the silicide coating.

The tee-stiffened panel was a welded sheet metal structure that required several more manufacturing operations than did the corrugated panel. However, the structure

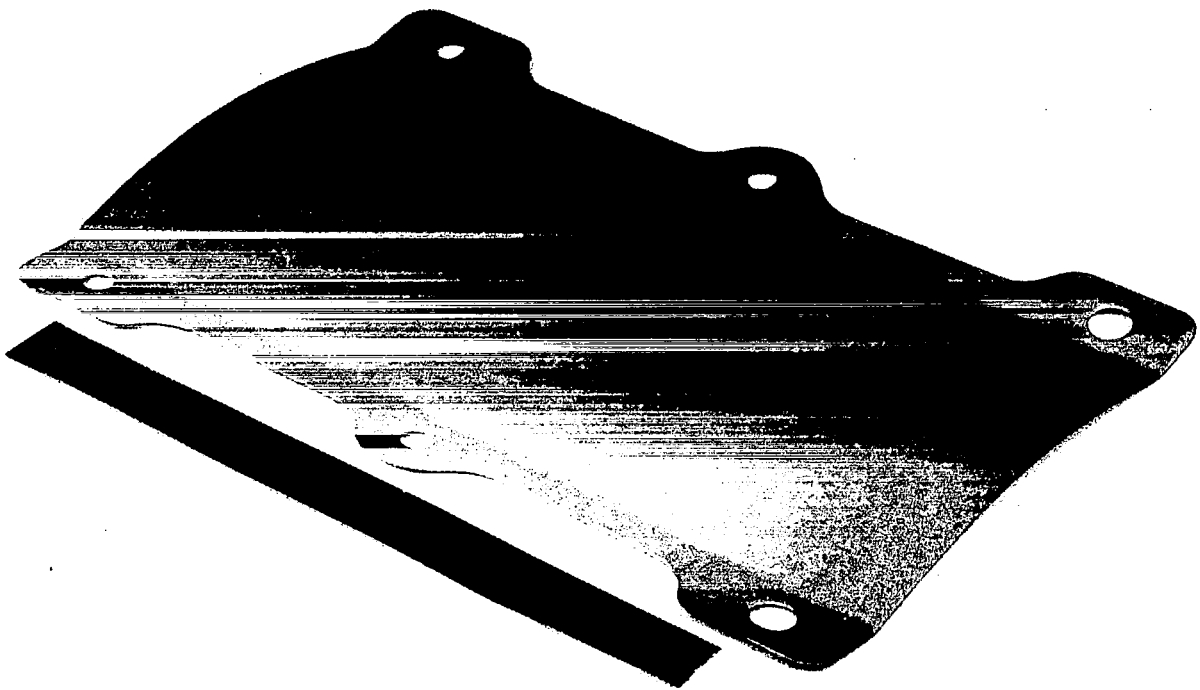


Figure 11. Exterior View of As-Coated Unexposed Subsize Corrugated Panel  
(Photo 123474)

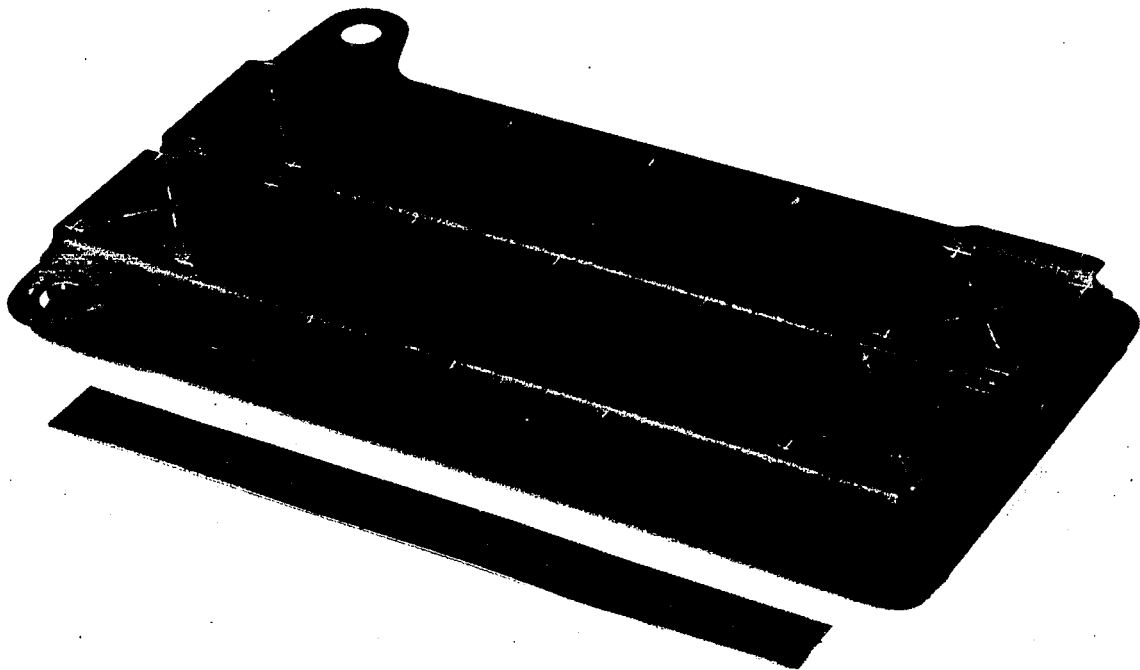


Figure 12. Interior View of As-Coated Unexposed Subsize Tee-Stiffened Panel  
(Photo 123471)

employed normal sheet metal fabrication. Only the edge and corner preparation and the use of electron beam welding differentiates this structure from other common sheet metal structures. The requirements for edge and corner preparation for coating were the same as for the corrugated panel. The edge preparation noted in figure 13 was sequenced to be done when the operation could be most readily performed during assembly (i. e., in detail or at some stage of assembly).

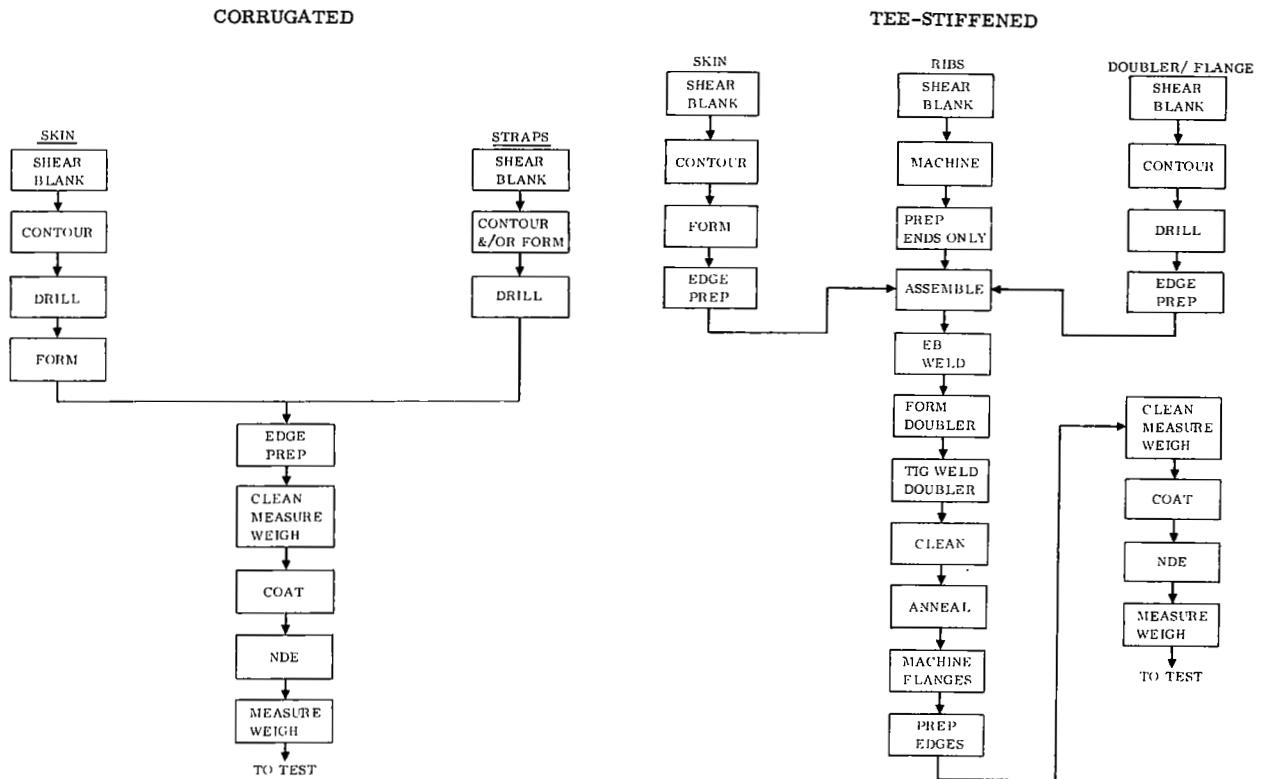


Figure 13. Fabrication Sequence for Subsize TPS Panels

Figure 14 graphically portrays the assembly, welding, and final forming operations for the tee-stiffened panel. It can be seen that the primary electron beam welding was done with the doublers in a flat and unformed position. This permitted access to the interior of the panel from either end for removal of internal weld tooling, for the inspection of the penetration side of the welds, and/or for the repair of the welds. After completion of the electron beam welding, the doublers were formed down, creating the panel end angles that were then tungsten inert gas (TIG) welded to the ends of the skin.

The electron beam welds were specified to be burn-through welds with 100% penetration, 100% root fusion of the flange, and fillets on each side of the vertical web or

rib. The TIG welds were required to have 100% fusion with no unfused regions permitted at the juncture of the doubler tabs and the skin.

The tooling philosophy for electron beam welding of the tee-stiffened panels was 100% solid, hard tooling (aluminum and chrome-plated copper). This required that all elements of the panel be assembled and located in the tooling before electron beam welds were made and all welds be accomplished without removing the panel from the tooling. Upon completion of the welds, the tooling was removed permitting inspection of both sides of all welds. When rewelding or repair welding was necessary, the tooling was reassembled on the part before welding. A limited number of interior repair welds were made without the aid of internal tooling. The TIG welds were performed without

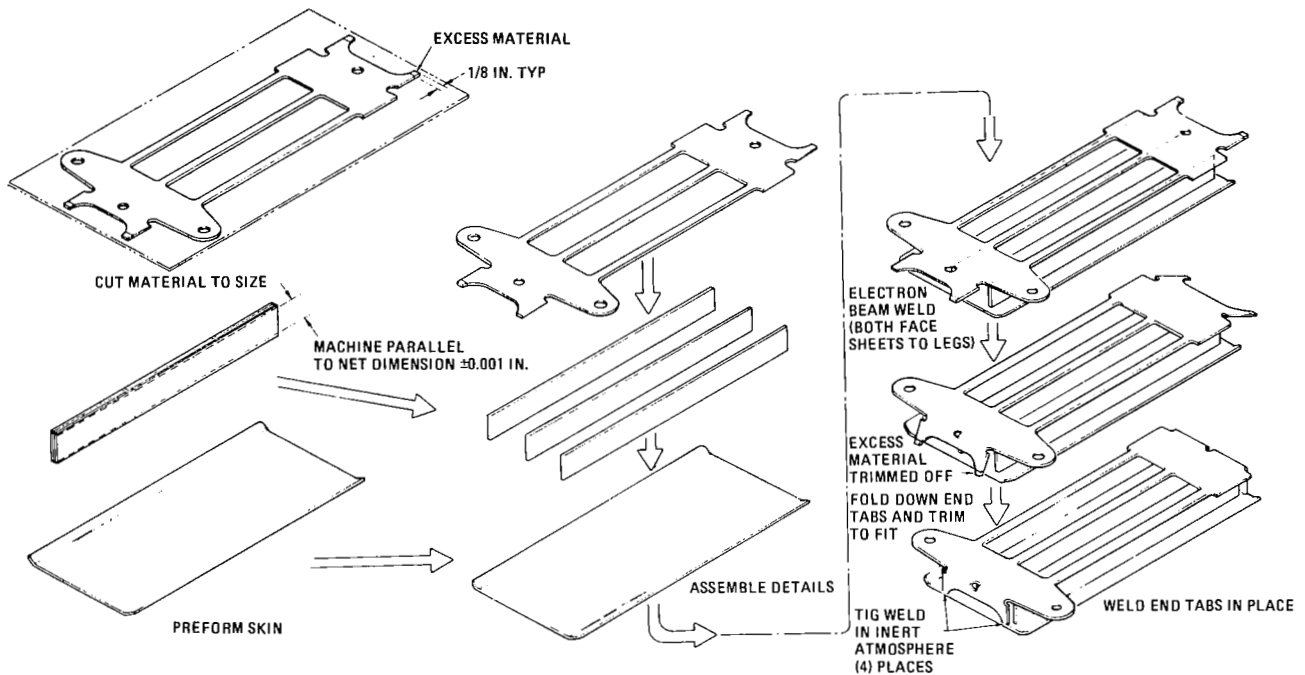


Figure 14. Subsize Tee-Stiffened Panel Fabrication Sequence

weld tooling and were made manually in a controlled atmosphere chamber. Visual and penetrant inspection techniques were employed to determine the quality of the welds.

Final annealing of the welded panels was done at 1590 K (2400°F) in a vacuum heat-treating furnace. Pressures less than  $6.67 \text{ MN/m}^2$  ( $5 \times 10^{-5}$  torr) were maintained. For protection from possible contamination during heat treatment, the panels were individually wrapped in tantalum foil.



The R-512E silicide coating was applied to the columbium alloy hardware following chemical or mechanical cleaning. Chemical cleaning was accomplished in a HNO<sub>3</sub>-HF acid solution, and mechanical cleaning was by grit blasting with iron particles. The coating slurry was applied by dipping and spraying with all edges overcoated or beaded using a miniature striping roller. Spray overcoating was employed on edges when the geometry of a part prevented using the striping roller.

### Panel Testing

The temperature profile described in figure 4 was used for the subsize panels. Applied loads simulating the pressure differential ( $\Delta p$ ) loading resulted in nominal stress levels as shown in table V.

TABLE V  
NOMINAL APPLIED STRESS LEVELS FOR SUBSIZE PANELS

$\Delta p$		Tee-Stiffened		Corrugation	
kN/m <sup>2</sup>	psi	MN/m <sup>2</sup>	psi	MN/m <sup>2</sup>	psi
20.7	3.0	91.6	13 287	133.5	19 357
13.8	2.0	61.1	8 858	89.0	12 906
1.03	0.15	4.6	664	6.7	968
3.10	0.45	13.7	1 993	20.0	2 904
5.86	0.85	26.0	3 765	37.8	5 485

A total of 10 subsize panels was tested in flight simulation exposure. The results are summarized in table VI. These panels received 964 total cycles with all but one completing the target of 100 cycles. Examples of the tee-stiffened and open corrugation subsize panels after 100-cycle exposure are shown in figures 15 and 16.

Results of the flight simulation exposure testing clearly demonstrated the capability of one of the material systems, Cb-752/R-512E, to sustain the required 100 cycles in both corrugated and tee-stiffened panel configurations. At the completion of 100 flight cycles, creep deformation was slight and no coating failures or substrate erosion occurred in the central test regions. The excellent performance of the Cb-752/R-512E during the subsize panel test complemented its previous performance (no coating failures) during the elemental evaluations. Therefore, the Cb-752/R-512E combination was selected as the system to be used in the small size [30.5 by 40.6 cm (12 by 16 inches)] TPS.

TABLE VI

## FLIGHT SIMULATION TEST SUMMARY FOR SUBSIZE PANELS

Alloy	Coating	Configuration	Cycles
Cb-752	R-512E	Corrugated	100
Cb-752	R-512E	Corrugated	100
Cb-752	R-512E	Tee-stiffened	100
Cb-752	R-512E	Tee-stiffened	100
Cb-752	R-512E	Tee-stiffened	100
Cb-752	R-512E	Tee-stiffened	100
C-129Y	R-512E	Corrugated	100
C-129Y	R-512E	Corrugated	100
C-129Y	R-512E	Tee-stiffened	100
C-129Y	R-512E	Tee-stiffened	64*

\*Withdrawn from test

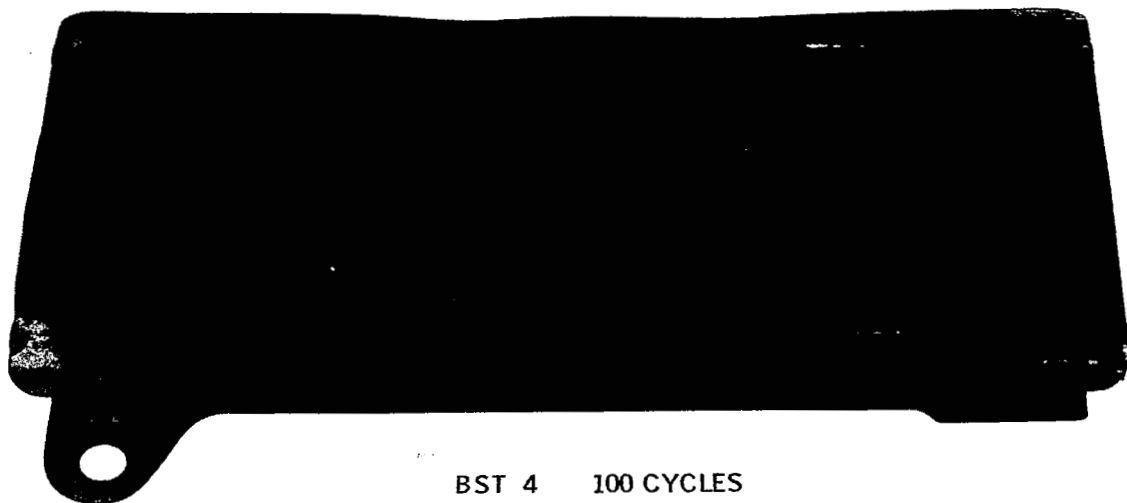
## SMALL SIZE TPS HARDWARE FABRICATION

The fabrication of test hardware for the metallic composite involved the use of a variety of conventional processes familiar to the aerospace industry. These included standard machining, electrical discharge machining, chemical milling, electron beam and resistance spot welding, vacuum brazing, heat treating, creep flattening, and standard sheet metal processing.

Figure 5 showed the corrugated TPS panel with retainer straps and posts atop the blanket of high temperature insulation and the support posts. All of the surface hardware and the upper half of the support posts were fully recrystallized Cb-752 coated with R-512E. The lower half of each support post was a high temperature nickel base alloy, Ni-20Cr-2ThO<sub>2</sub>. All fasteners were Ni-20Cr-2ThO<sub>2</sub>, except the two horizontal bolts and nuts for the corrugated configuration and the filler plugs in each post, which were Cb-752 and designed not to be removed.

Figure 17 shows the interior side of the heat shield on which may be seen the built-up brazed forward beam and the machined aft beam. Also visible are the two panel stiffeners running transverse to the corrugations and located under each beam. These stiffeners were produced by chemical milling of the panel skin.

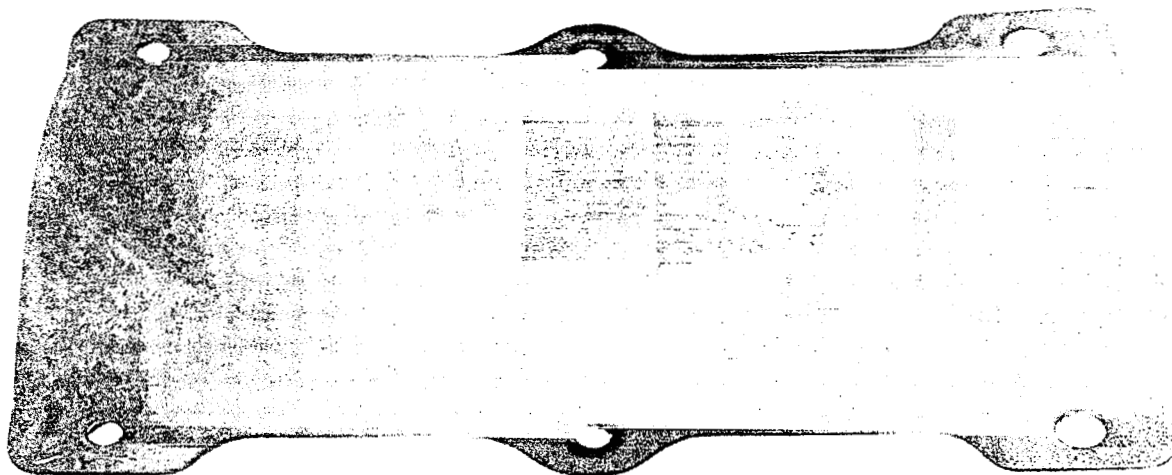
Figure 1 showed the tee-stiffened panel and retainers at the hot surface with the support posts and the insulation below. All the surface hardware, the top half of the support posts, and the filler plugs were Cb-752. The lower halves of the support posts and all fasteners were made of Ni-20Cr-2ThO<sub>2</sub>.



BST 4 100 CYCLES



Figure 15. Exterior View of Cb-752/R-512E Tee-Stiffened Subsize Panel after 100 Flight Simulation Cycles (Photo 12-2817)



BSC 2 AFTER 100 CYCLES



Figure 16. Exterior View of Cb-752/R-512E Open Corrugation Subsize Panel after 100 Flight Simulation Cycles (Photo 12-5719)

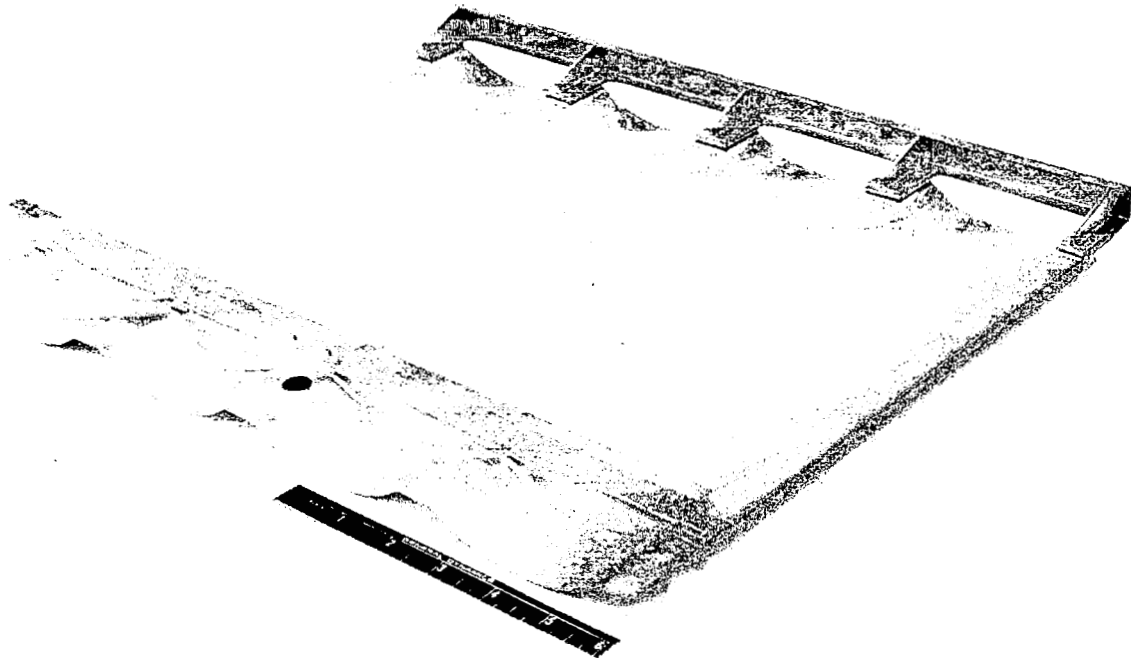


Figure 17. Interior View of Brazed Cb-752 Open Corrugation Heat Shield (Photo 12-6980)

Figure 18 shows a completed tee-stiffened heat shield panel ready for test. These panels were completely assembled by electron beam welding, each panel containing over 30 feet of weld applied without any straightening or intermediate heat treating of the parts. The panels were first welded into a subassembly composed of the skin, flange skin, and ribs, which was subsequently machined to receive the end closure beams for welding.

HiTemCo's R-512E silicide coating was used on all Cb-752 components and was applied as previously described for the subsize panels. All Ni-20Cr-2ThO<sub>2</sub> parts were coated with an aluminide to impart oxidation resistance and as a protective measure to minimize any incompatibility between the dispersion-strengthened metal and the silicide coating on the columbium alloy. This Cr-Co-Al-Y coating, designated VH-28, was applied by Vac-Hyd Processing Corporation.

The electron beam welding used on the tee-stiffened panels involved three types of weld joints: (1) burn-through tee-welds between ribs and skins and flanges, (2) step-butt welds between skins and flange skins and closure beams, and (3) burn-down tee-welds between rib tangs and beam webs. All webs required 100% joint fusion with full penetration and fillet formation. Welds were made using chrome-plated copper and aluminum hard tooling. Hard chromium was applied to copper tooling to prevent copper contamination of the columbium during welding and assembly operations. As further

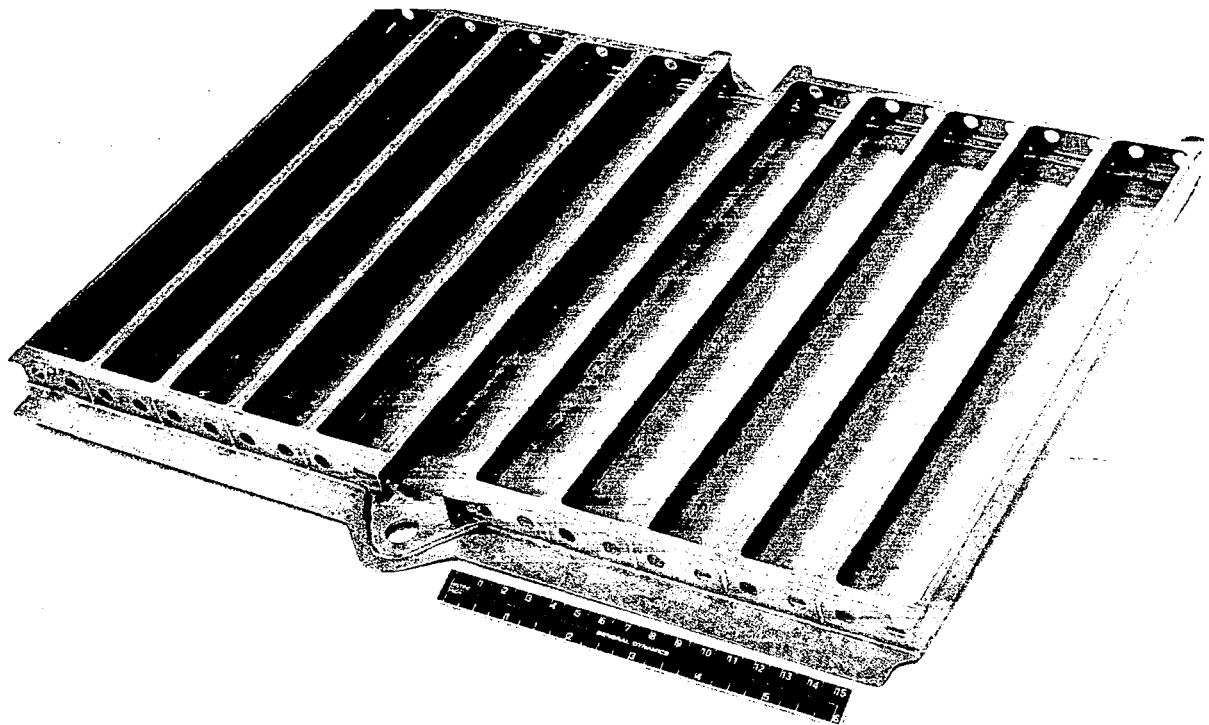


Figure 18. Interior View of Electron Beam Welded Tee-Stiffened Cb-752 Heat Shield (Photo 12-8326)

insurance, all parts were bathed in nitric acid to remove residual copper prior to each heating or welding operation.

All formed and welded parts were simultaneously annealed and creep flattened to assure stress free and properly fitting parts. This operation was performed at 1589° K (2400° F) for one hour in a vacuum of 6.67 MN/m<sup>2</sup> ( $5 \times 10^{-5}$  torr) or better. Parts were loaded with refractory metal weights to effect creep flattening during annealing.

Brazing was used extensively in the fabrication of the test hardware, especially for the corrugation stiffened panels. For these panels, it was the principal joining method. Brazing of the corrugated Cb-752 panels employed the use of Ti-33Cr braze alloy (ref. 10). Brazing was followed by a high temperature diffusion treatment. Due to the characteristics of the Ti-33Cr alloy, it was necessary to have metal-to-metal fits in all joints to assure satisfactory flow and filleting of the braze alloy. The joint fit-up and the braze alloy were held in position by resistance spot welding. Braze alloy was available only in foil form and was 0.052 mm (0.002 inch) thick.

Columbium alloy brazing was accomplished in a vacuum furnace under an atmosphere of high purity argon (<2 ppm O<sub>2</sub>) by heating to 1590 K (2400° F) and stabilizing for five minutes followed by a temperature increased to 1760 K (2700° F) and an eight-minute hold at temperature.

After brazing, the parts were either furnace cooled to room temperature or cooled with high purity argon or helium at temperatures below 530 K (500° F). Simple, light-weight molybdenum tooling was used to hold and support parts during brazing.

After brazing, the columbium parts were diffusion treated by heating at 1590 K (2400° F) in a vacuum for a period of 16 hours. During the diffusion treatment, the parts were protected from possible contamination from the furnace atmosphere during the long time at temperature by wrapping with tantalum foil. Cooling was similar to that that used for brazing.

Brazing was also used to fabricate the Ni-20Cr-2ThO<sub>2</sub> lower support posts, which were common to both TPS configurations. The brazing of Ni-20Cr-2ThO<sub>2</sub> permitted the joining of the flange to the main body of the lower support posts. This involved conventional vacuum brazing at 1560 K (2350° F) for approximately four minutes. TD-6 (Ni-16Cr-4Si-5W-17Mo) was used as the braze alloy.

### SMALL-SIZE TPS TESTING

To further evaluate the two TPS configurations, now that the material system selection had been made, two separate test series were undertaken. The first was conducted in a hot gas flow facility to investigate the system structural integrity and leakage effects. The second was conducted in a radiant heat chamber to investigate the system response while undergoing temperature, pressure differential loading, and local surface pressure conditions. All specimens also were exposed to representative acoustic excitation before and after thermal testing.

#### Thermal Flow Testing

The flow-test specimens, each mounted in a copper, water-cooled holding frame, were installed in a shroud test section that provided for a flat flow channel across the heat shield surface (fig. 19). For the test profile the combustion was controlled with a near stoichiometric mixture ratio of 8/1 to 8.3/1 by weight of O<sub>2</sub> and H<sub>2</sub>. Each of these two specimens was to be cycled through the test profile 20 times at these one atmosphere oxidizing conditions, which was judged to be the equivalent of 100 reduced pressure thermal cycles.

Open corrugation TPS. - The test specimen shown in figure 19 was cycled 10 times at cold wall heating rates up to 780 kW/m<sup>2</sup> (69 Btu/ft<sup>2</sup>), which produced nominal peak heating surface temperatures of 1590 K (2400° F). The temperature corrected maximum nominal velocity was M=0.8 and the flat plate static pressure at peak temperature was 172 N/m<sup>2</sup> (0.025 psig). During the inspection after cycle 10 the leading edge of the main heat shield was found to have separated from the forward auxiliary panel. The

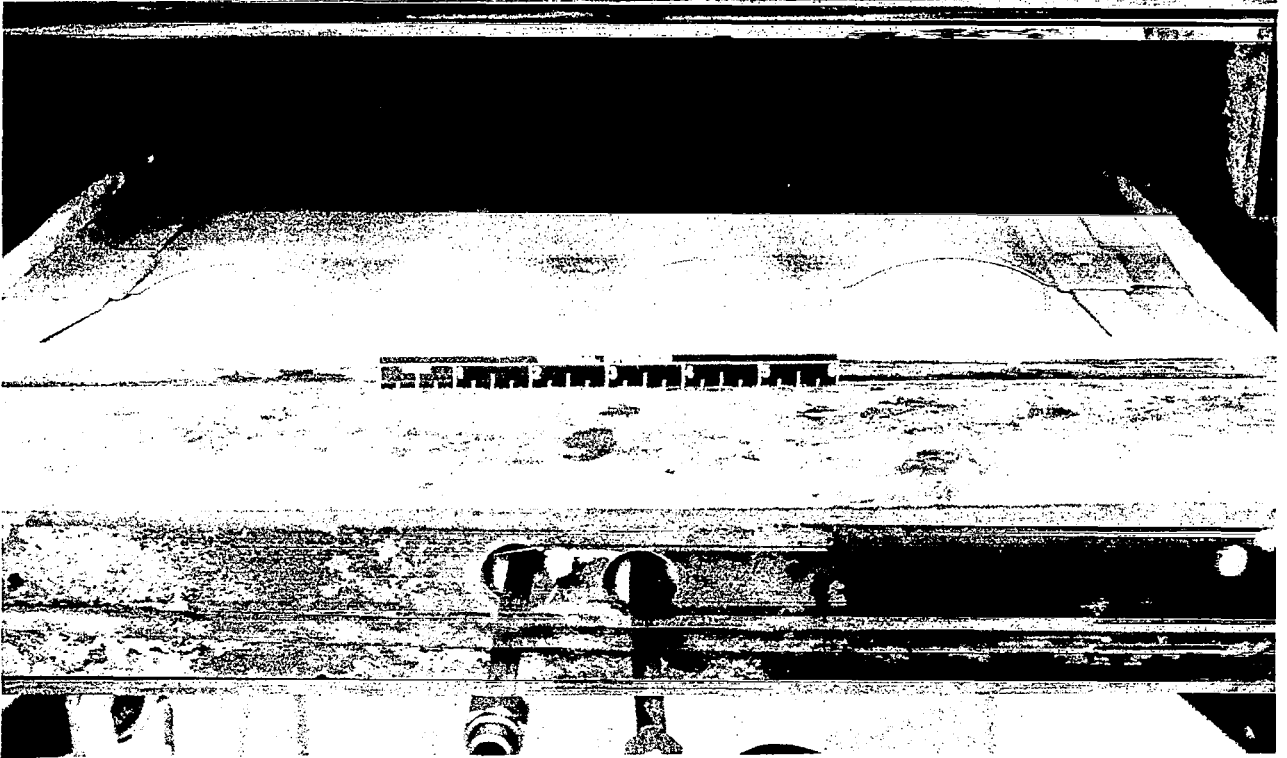


Figure 19. Open Corrugation TPS Specimen Installed in Hot Gas Flow Facility Prior to Testing (Photo 13-2620)

panel had sustained local damage that required partial specimen disassembly and repair. This afforded an opportunity to conduct field repair and to determine the degree of reusability resulting from this practice.

The specimen was disassembled with relative ease by removing the Cb-752 plugs, Ni-20Cr-2ThO<sub>2</sub> bolts and Cb-752 retainers. The heat shield was repaired using the glass frit method of reference 12. After reassembly testing was resumed for the remaining 10 cycles. The damage sites exhibited no further oxidation or crack propagation after being repaired. The practicality of in-place or field repair was thus demonstrated.

It is important to note that following the heat shield repair, the facility malfunctioned twice. The malfunction produced surface temperatures in excess of 1760K (2700° F) for four minutes during one cycle and approximately 1730K (2650° F) for three minutes during another. Structurally no detrimental effects were found due to these temperature excursions, thereby indicating a comfortable overshoot capability for the coated columbium alloy material system.

A composite temperature distribution is shown in figure 20, which illustrates the degree of predicted accuracy when compared with the recorded data. Similar accuracy was achieved for the tee-stiffened TPS specimen.

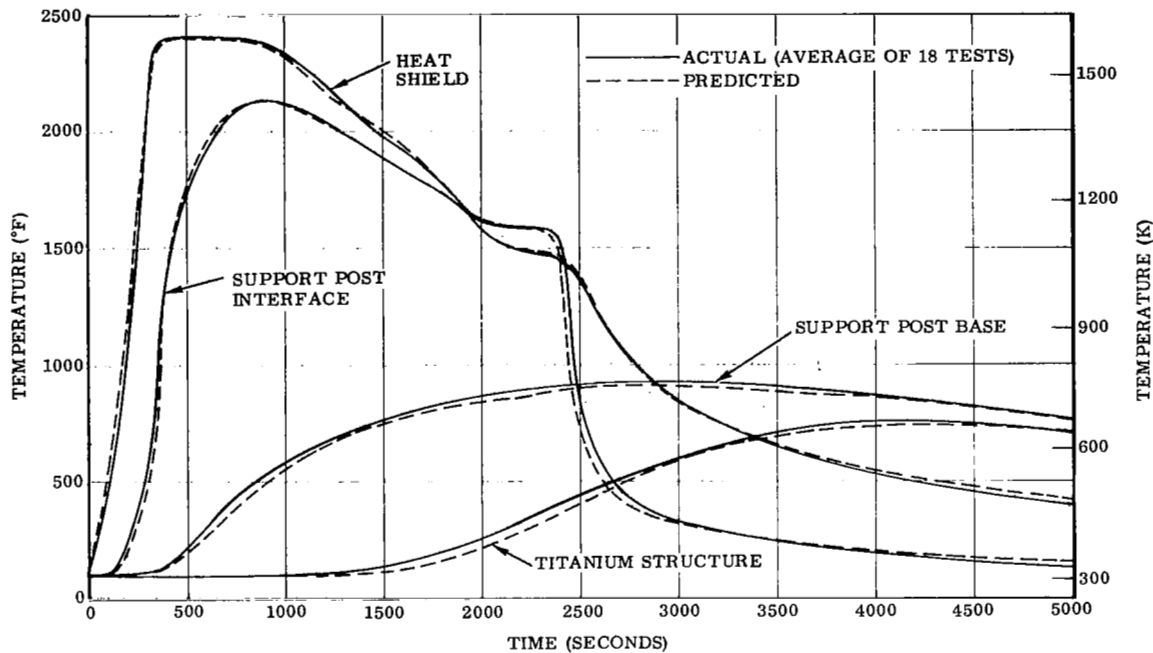


Figure 20. Hot Gas Flow Test Composite Temperature Distribution - Open Corrugation TPS

Tee-stiffened TPS. - The tee-stiffened TPS specimen (fig. 21) was also subjected to 20 thermal flow cycles. The maximum heating rate was  $680 \text{ kW/m}^2$  ( $60 \text{ Btu/ft}^2 \text{ sec}$ ) and the total mass flow rate was  $0.118 \text{ kg}$  ( $0.259 \text{ lb}$ ) per second. The static pressure and the Mach number were  $170 \text{ N/m}^2$  ( $0.025 \text{ psig}$ ) and  $0.8$  respectively. No anomalies were experienced during this test series. The specimen was removed and partially disassembled after cycle 10 as previously described. Disassembled components are shown in figure 22.

Hot gas flow test summary. - In comparing the hot gas flow test performance of the open corrugation and tee-stiffened TPS specimens, little differentiation could be found. The material systems performed well with no coating failures on either specimen (with the exception of the mechanically induced edge defect on the corrugation specimen). No post-test structural defects were found in the tee-stiffened specimen. The structural difficulty encountered with the corrugation specimen was believed to have been induced by an improperly assembled specimen. In addition there is some reason to suspect the quality of the forward beam brazement. The insulation performed well and appeared to be unaffected by hot gas leakage into the system or by moisture due to humidity.



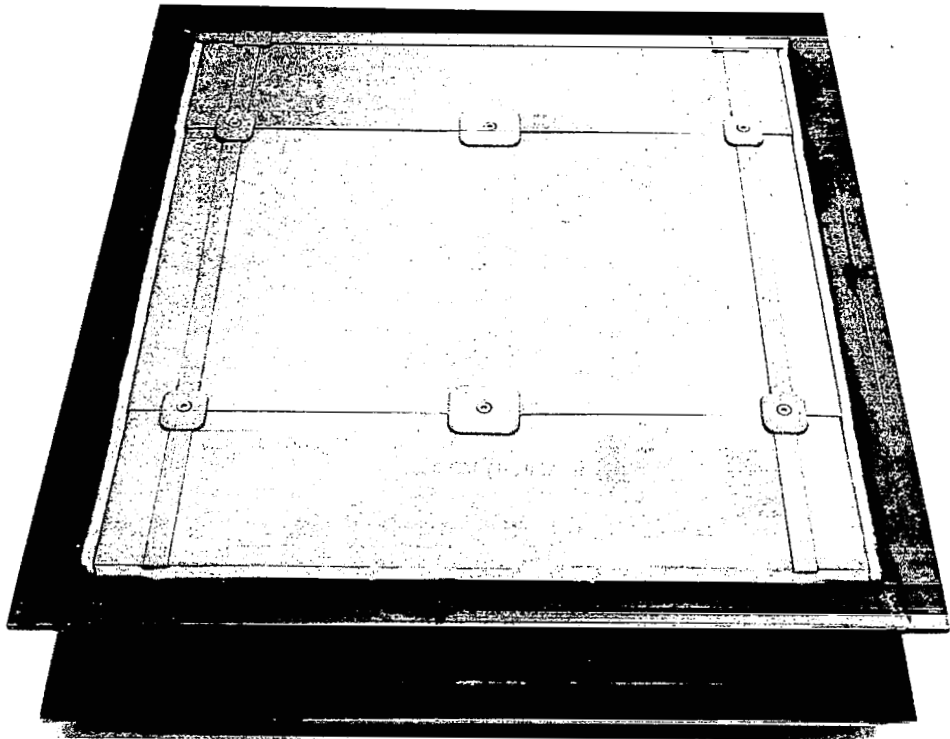


Figure 21. Unexposed Tee-Stiffened TPS Specimen – End View (Photo 13-0328)

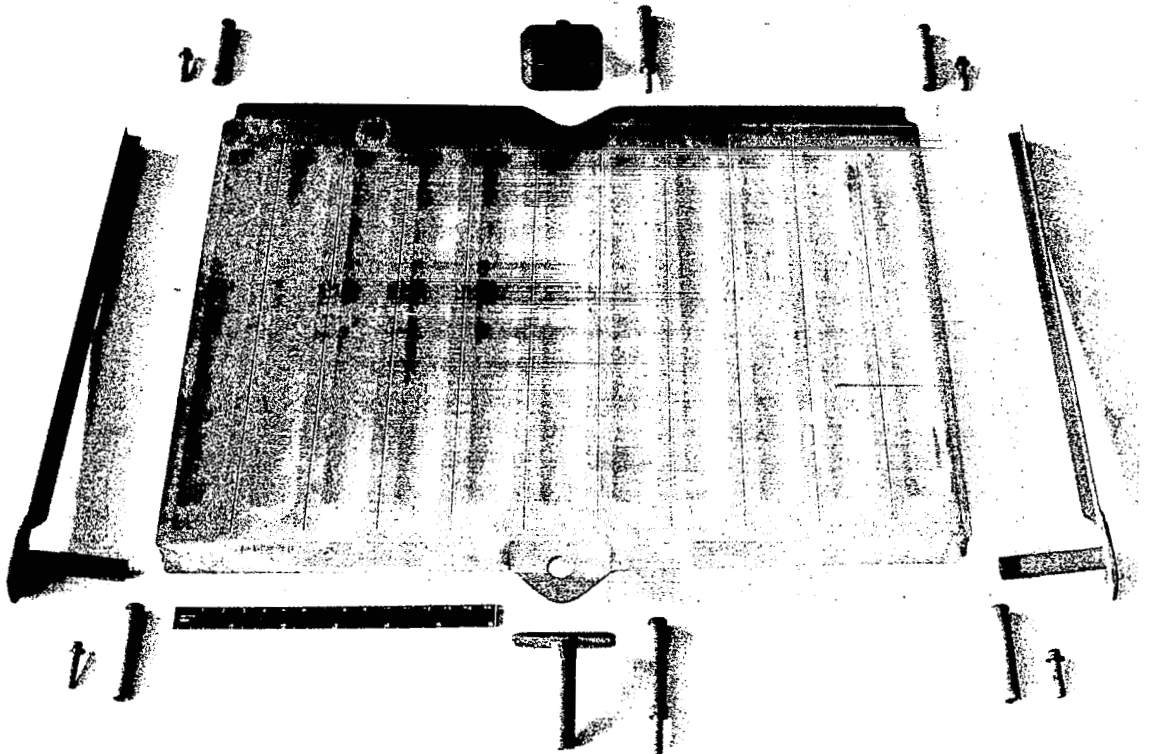


Figure 22. Tee-Stiffened Heat Shield (Exterior Side) and Attachments after 20 Hot Gas Flow Thermal Cycles and 100 Acoustic Cycles (Photo 13-3768)

## Radiant Heat Testing

Each specimen designated for radiant heat testing with applicable pressure differential loading and reduced pressures was housed in a stainless steel holding fixture and mounted with the heat shield surface in a down position. Each test began with the maximum evacuation of the chamber to maintain the required chamber pressure and pressure differential across the face of the heat shield. Following the boost phase of the profile the specimen required approximately one hour to return to a maximum internal temperature of less than 310 K (100° F). The entry phase of the profile began with the chamber fully evacuated and the pressure was increased by bleeding in air/nitrogen at a controlled rate and mixture to maintain the required surface pressure. At the conclusion of each cycle, the chamber was backfilled to ambient pressure with GN<sub>2</sub>. Cycling was resumed when the maximum recorded internal temperature at the center of the insulation was less than 310 K (100° F). The chamber was opened approximately every 10 cycles for specimen inspection until the completion of 50 cycles.

Open corrugation TPS. – No unusual conditions were observed as a result of the radiant heat tests. The specimen evidenced no sign of coating failure, substrate erosion, or structural degradation. The specimen exhibited a non-uniform pattern of coloration. As with all previous specimens (elemental and subsize panels) the random coloration was not deleterious to the system performance.

The temperature measurements for the entire test series showed good temperature uniformity over the surface of the specimen. The average maximum temperature at the center of the heat shield surface was 1590 K (2400° F), which was the programmed temperature. The bi-metallic post interface temperature maximum was 1450 K (2149° F) versus a predicted peak of 1450 K (2150° F). The maximum average temperature at the base of the Ni-20Cr-2ThO<sub>2</sub> post was 757 K (921° F) compared to a predicted value of 764 K (915° F). The average temperature maximum at the center of the titanium skin was 671 K (747° F) compared to a predicted level of 672 K (750° F). After completion of the 50 thermal cycles the specimen was subjected to 75 simulated boost acoustic cycles.

Tee-stiffened TPS. – Similar to the open corrugation TPS test series the specimen experienced a uniform temperature distribution with the peak heat shield temperatures ranging from a minimum of 1586 K (2395° F) to a maximum 1594 K (2410° F). The maximum average temperature at the Cb-752/Ni-20Cr-2ThO<sub>2</sub> support post interface was 1452 K (2153° F) compared to a prediction of 1450 K (2150° F). The support post base experienced an average peak temperature of 771 K (927° F) compared to a predicted level of 764 K (915° F). The actual support structure skin temperature exceeded the prediction by 5 K (7° F) attaining an average of 676 K (757° F).

The specimen is shown in figure 23 after 50 thermal cycles. Again, the varied surface patterns can be seen in the post test photographs. No sites of substrate oxidation,

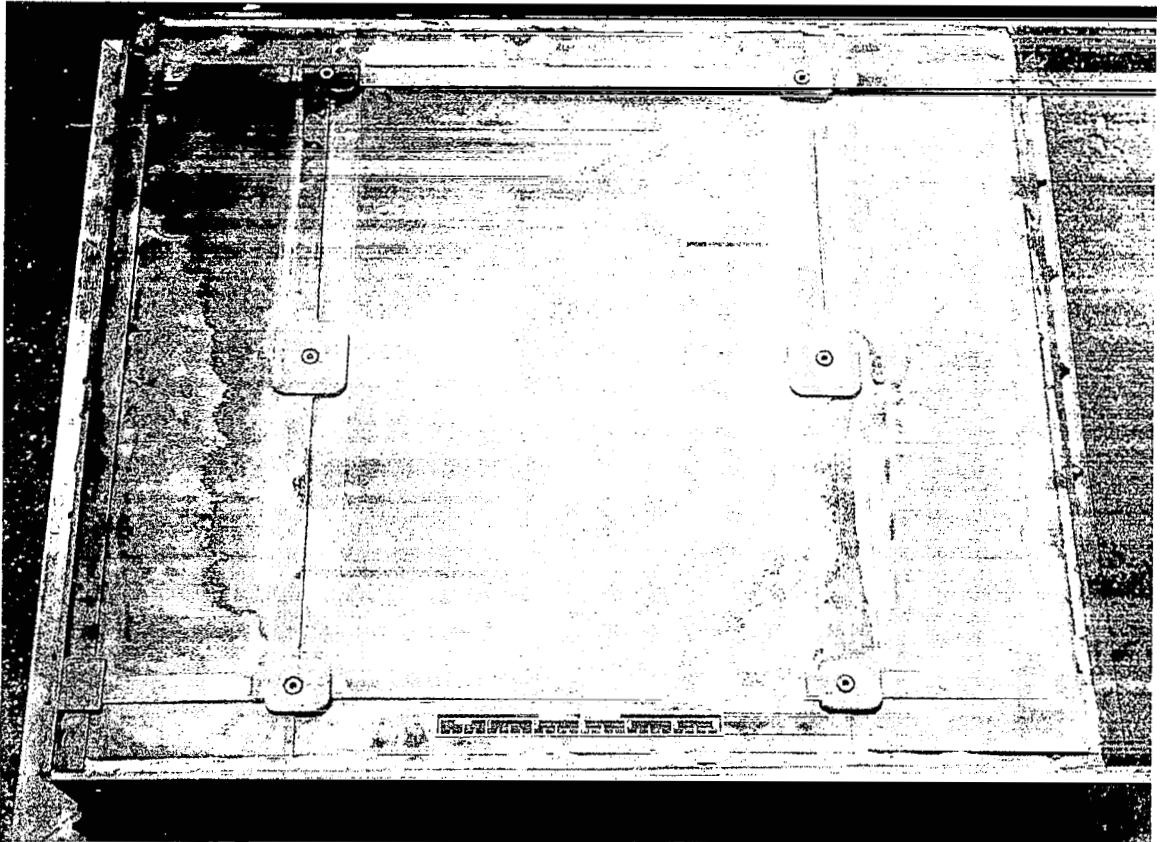


Figure 23. Tee-Stiffened TPS Specimen after 50 Radiant Heat/  
Pressure/Load Cycles – Side View (Photo 13-2766)

impending coating failure, or structural deterioration were found. Following the 50 thermal cycle exposure the specimen was exposed to 75 simulated boost acoustic cycles.

Radiant heat test summary. – Both types of specimens performed well during the radiant heat test series. The temperature distributions through the depth of the specimens were near the predicted levels. No structural failures were found on either specimen. The concept of sliding, coated surfaces did not cause any difficulties; that is, no excessive wear appeared in those regions of overlap. In addition, the concept of buried fasteners provided for relatively easy panel and insulation inspection. No incompatibility between the silicide coated columbium alloy and the aluminide coated Ni-20Cr-2ThO<sub>2</sub> was found.

Based on this test series no clear preference could be made between the two configurations. Therefore, the selection of the tee-stiffened TPS as the system for Phase III evaluation was based on its slightly lower unit weight and cost and the general preference for fabricating using electron beam welding instead of brazing.

## Acoustic Testing

The objective of the acoustic test series was to determine the structural response of each of the two TPS configurations to acoustic excitation at representative boost noise levels. All specimens were mounted vertically in their respective holding fixtures through the side wall of a reverberation chamber. Dynamic response was measured with miniaturized accelerometers attached to the external surface of the heat shield. Each of the four specimens was subjected to an acoustic cycle consisting of an overall sound pressure level (OASPL) of 155 dB for 10 seconds followed by an OASPL of 152 dB for 40 seconds. The test sequence for the entire test series was:

<u>Radiant Heat Test Specimens</u>	<u>Hot Gas Flow Test Specimens</u>
Acoustic test (25 cycles)	Acoustic test (1 cycle)
Disassemble and inspect	Disassemble and inspect
Thermal test (50 cycles)	Thermal test (20 cycles)
Acoustic test (75 cycles)	Acoustic test (99 cycles)
Disassemble and inspect	Disassemble and inspect

No phenomena detrimental to the thermal/structural performance of the tee-stiffened TPS were observed at the test conclusion. Several areas of rubbing were seen at locations where adjacent panels, posts, and retainers were in contact. A fine powdered surface was created by a wearing down of the unsmooth surface of the coating. This powder could be removed by light brushing. No preferential oxidation of the substrate was found at these regions during post-test inspection.

The specimens were disassembled twice, after 25 and 100 cycles for the radiant heat test specimen and after 1 and 20 cycles for the hot gas flow exposed specimen. No difficulty was encountered during the disassemblies. The breakaway torque to remove the Cb-752/R-512E plug from the coated Ni-20Cr-2ThO<sub>2</sub> bolt ranged from 191 to 259 cm-N (17 to 23 in-lb) compared to the applied setting torque of 147 cm-N (13 in-lb). The Ni-20Cr-2ThO<sub>2</sub> bolts were removed from the Cb-752/R-512E support post by applying between 191 and 270 cm/N (17 and 24 in-lb) of torque. The initial setting torque was 169 cm/N (15 in-lb). No significant differences were noted in the removal qualities with regard to type of thermal test or exposure duration.

## FULL-SIZE TPS

Following the selection of the tee-stiffened heat shield configuration of the previous study phase, the final evaluation involved enlarging the total specimen and ensuring complete isolation of a single test panel plus representative adjacent panels. The size of the individual heat shields remained 30.5 by 40.6 cm (12.0 by 16.0 inches). The total array was 103.9 by 137.0 cm (40.9 by 54.0 inches). Including the simulated primary structure, the thickness was 16.3 cm (6.4 inches) of which the TPS consisted 11.07 cm (4.36

inches). The titanium primary structure heat sink consisted of a 0.051 cm (0.020 inch) skin, two 0.203 cm (0.080 inch) I-frames at 30.5 cm (12.0 inch) spacing, and five rows of 0.051 cm (0.020 inch) Z-stringers.

Minimal design modifications were made to the full-scale hardware between Phases II and III. The changes were generally made to reduce material costs, to improve fabrication efficiency, or because of material scarcity. Extensive use was made of electron beam welding to reduce weight and material costs and to minimize machining operations. The lower temperature portion of the bi-metallic support posts was changed from Ni-20Cr-2ThO<sub>2</sub> to the cobalt-base alloy HS-25 (Co-10Ni-20Cr-15W-3Fe). This change was necessitated by the unavailability of Ni-20Cr-2ThO<sub>2</sub> bar stock at the time of component fabrication. The blanket insulation material was changed from Dyna-Flex to Fiberfrax H. This material, as received, had an average thickness of 0.84 cm (0.33 inch) and a calculated density of 91 kg/m<sup>3</sup> (5.7 lb/ft<sup>3</sup>). This was compressed to 114 kg/m<sup>3</sup> (7.1 lb/ft<sup>3</sup>) upon installation and compares to the as-installed density of 192 kg/m<sup>3</sup> (12 lb/ft<sup>3</sup>) of Dyna-Flex. The insulation material change was due to the desire to increase the system thermal efficiency, reduce the unit weight, increase the ease of handling after exposure, and to have a material that did not contain a binder. All of these goals were achieved with the use of Fiberfrax H.

### Testing

The objective of the final test program was to functionally test a full-scale, vehicle-sized, thermal protection system test specimen consisting of heat shields, panel retainers and supports, close-outs, and insulation, and to evaluate the effects on the system of simulated Shuttle Orbiter missions.

The test conditions for the nine-panel array were 50 cycles of simulated flight environment with boost and reentry times, temperatures, pressure loads, oxygen partial pressures, and 100 cycles of acoustic fatigue. Since the maximum acoustic excitation and associated potential damage were predicted to occur during boost and with minimal temperature considerations, testing was accomplished in three steps. First, the specimen was acoustically tested at ambient temperature through 50 simulated boost cycles of noise, followed by 50 simulated flight thermal cycles. Finally, the specimen was again exposed to 50 simulated boost cycles of noise at ambient temperature. This represented a conservative approach with the specimen repeatedly acoustically loaded to maximum levels, after having sustained the full-term effects of 50 thermal cycles.

The full-size TPS array representing a portion of the Shuttle Orbiter underbody heat shield was designed for testing based on the evaluation of the results of Phase II. The design satisfied vehicle requirements for location, loading, and frame spacing. The specimen consisted of a rectangular array of nine tee-stiffened heat shield panels (three panels long by three panels wide) with 10 panel support posts, six fixed-point panel center retainers, six panel edge retainers, and high temperature insulation, all mounted

on a simulated vehicle load-carrying structure of titanium skin, frames, and stringers. A water-cooled HS-188 test specimen support frame enclosed the nine panels and supported the load structure. The nine-panel arrangement permitted the complete isolation of the center panel, affording freedom from the test frame edge effects. It also allowed the inclusion and testing of a variety of panel edge restraints that are normal to flight hardware. The assembled test specimen is shown in figure 24 prior to testing.

Pre-thermal acoustic testing. - Acoustic testing of the nine-panel test specimen was performed in a 3.6 m<sup>3</sup> (128 cu ft) reverberation chamber with the test array mounted vertically in the wall, with apparent air flow going from the top of the specimen toward the bottom. The specimen was supported from the rear and was vibration isolated from the acoustic chamber structure. It was mounted so that only the external surface of the columbium alloy heat shields was subjected to direct acoustic excitation. The center of the array was instrumented with nine miniature accelerometers to record the response of the panel and panel retainers to the acoustic flight environment.

Before boost simulation testing was started, the specimen was subjected to a low level sinusoidal sweep from 50 to 1000 Hz to determine the resonant frequencies of each accelerometer position and the phase relationship referenced to an accelerometer mounted on the test fixture frame. The specimen was then subjected to 50 cycles of boost simulation, each cycle composed of 10 seconds at an overall sound pressure level (OASPL) of 158 dB followed by 40 seconds at 155 dB OASPL. Visual inspection of the specimen was performed at least once each 10 cycles during cycles 1 to 50 and at least once every five cycles thereafter. Figure 25 details the noise environment expected during shuttle boost and an actual test spectrum. No structural damage was sustained as a result of this test.

Thermal-mechanical testing. - After completion of 50 cycles of acoustic testing, the nine-panel test specimen was mounted in the high temperature testing facility seen in figure 26 and shown schematically in figure 27.

This facility consisted of two box-like, stainless steel enclosures: the bottom enclosure that mounted the test specimen and temperature sensing instruments, and the top enclosures that mounted the power distribution system, the heat lamps, the cooling air distribution system, the pressurization gas and oxygen partial pressure manifolding, and the hot air plenum and exhaust ducting. The top enclosure was insulated with approximately 5 cm (2 inches) of fused silica foam insulation (Glasrock) that was mechanically mounted. An oxygen partial pressure sensor line was also mounted in the top enclosure. The two enclosures were hinged to open in a clam-shell fashion exposing the skin surfaces of the test specimen. Opening was accomplished by two hydraulic cylinders operated from an air-hydraulic accumulator. The two surfaces closed and sealed against a silicone rubber gasket, permitting pressurization of the cavity over the specimen.

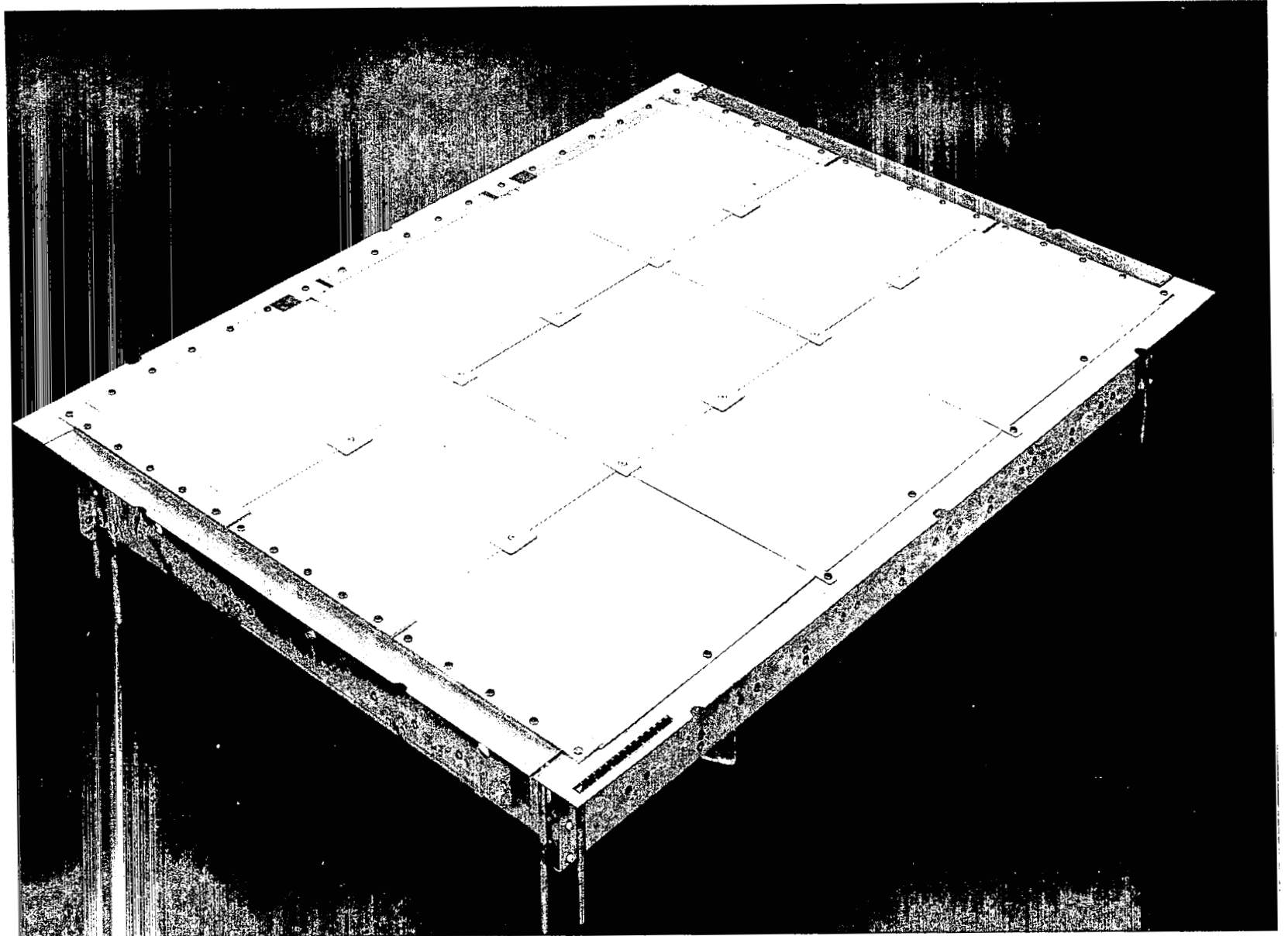
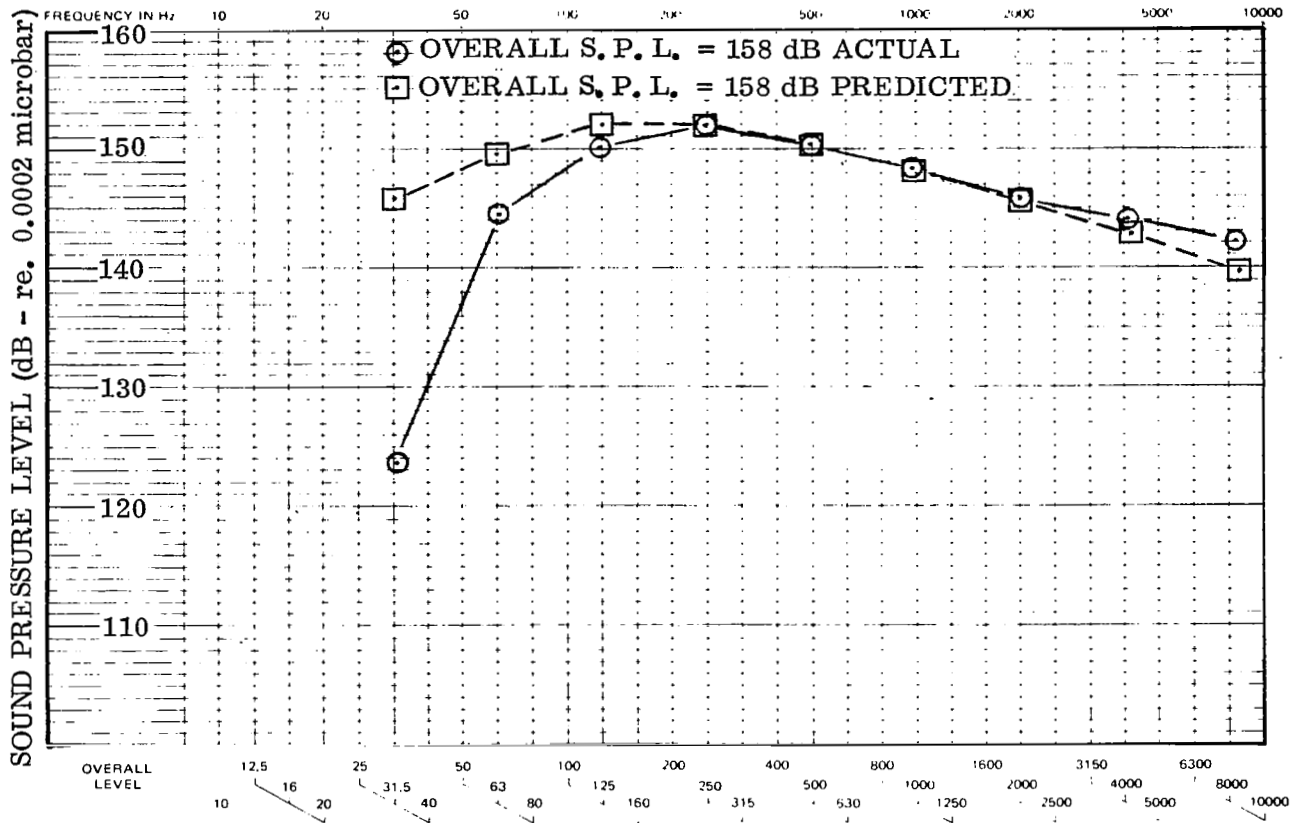


Figure 24. Assembled Test Specimen Prior to Testing (Photo 13-7397)



1/3 OCTAVE AND OCTAVE BAND CENTER FREQUENCIES  
 Figure 25. Acoustic Spectrum – High Level (Pre-Thermal Tests)

Before the start of the reentry portion of the test cycle, the plenum was flooded with nitrogen gas until the oxygen content approached zero. During reentry, the amount of oxygen in the nitrogen atmosphere was increased with time, controlled by metering air through solenoid operated orifices, thus providing in a stepped function the desired oxygen content and oxygen partial pressure over the test specimen. The automatic four-step metering of oxygen into the mixture provided a good approximation of the desired oxygen content during reentry with the mixture being evenly distributed over the surface of the specimen.

Fifty thermocouples were installed in the test specimen to acquire thermal profile data during test cycles. Of these, 14 were tungsten/rhenium (W-5 Re/W-26 Re) sheathed thermocouples that were spring loaded against the back of the hot face of all nine test panels. Thirty-six were chromel-alumel thermocouples installed to measure temperatures of the support posts, the titanium skin cold face, and the insulation.

When the nine-panel test specimen became available and was installed in the high temperature simulation flight test facility, pressurization tests were run to determine



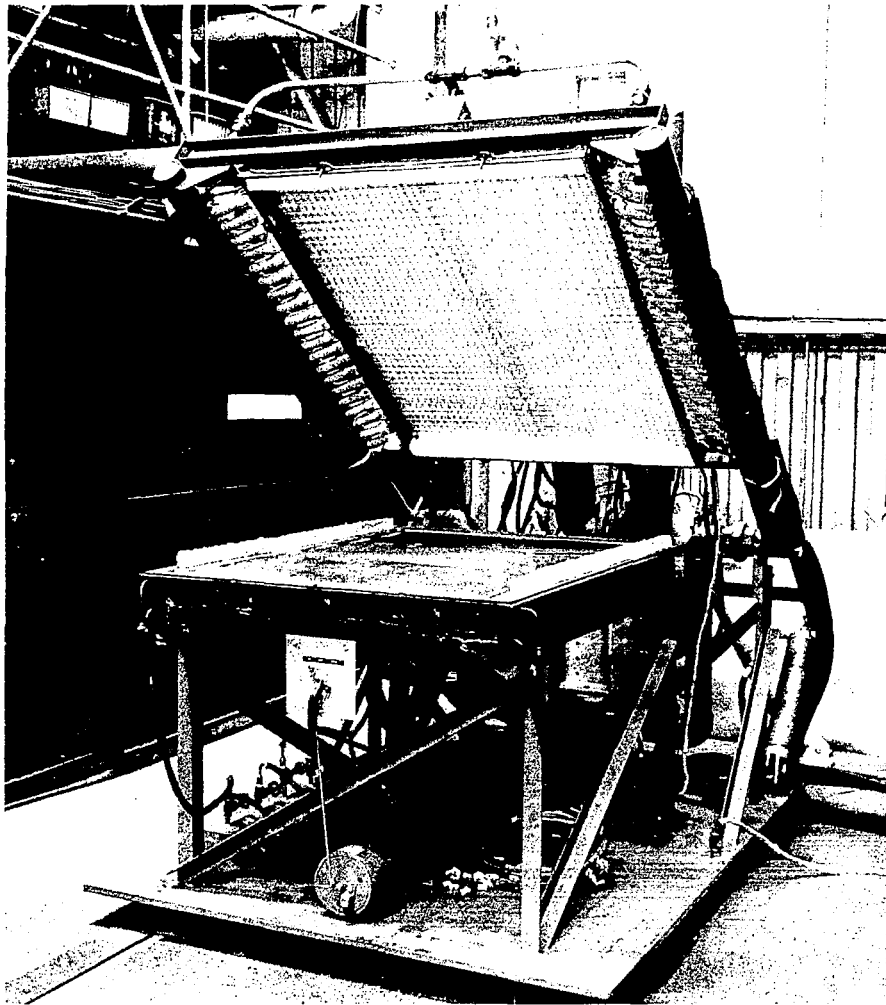


Figure 26. Facility for Thermal, Load, and Environmental Testing of Multi-Panel TPS (Photo 135429)

the pressure loading capability of the test system. From figure 4 it can be seen that the maximum required test pressure during boost was  $21 \text{ kN/m}^2$  (3.0 psi), and  $1.0 \text{ kN/m}^2$  (0.15 psi) during high temperature reentry. Pressurization tests indicated that for a pressure of  $7.45 \text{ kN/m}^2$  (1.08 psi),  $0.10 \text{ m}^3/\text{sec}$  ( $220 \text{ ft}^3/\text{min}$ ) of air was required. Thus for  $21 \text{ kN/m}^2$  (3.0 psi) an intolerably high flow rate was indicated. Pressure testing was performed that isolated the specimen and the facility and that showed that 56% of the apparent leaks were around the specimen holding fixture and through the test specimen. The balance of the losses were through the top enclosure around the quartz cooling tube penetrations and the quartz tube penetrations into the hot gas plenum.

Continued testing at decreasing pressures indicated that to attain the desired reentry pressure of  $1.0 \text{ kN/m}^2$  (0.15 psi), a gas flow of  $0.026 \text{ m}^3/\text{sec}$  ( $55 \text{ ft}^3/\text{min}$ )

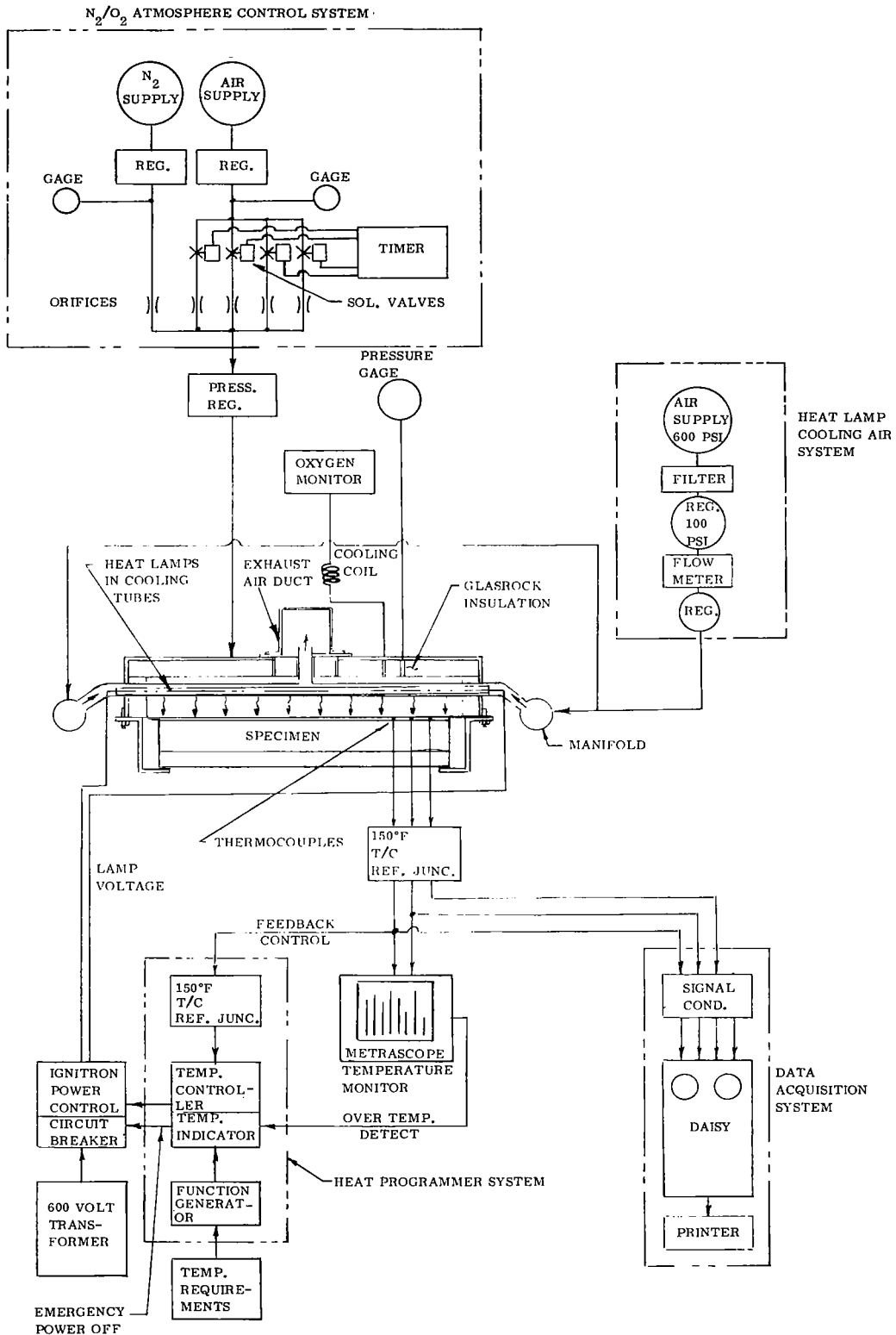


Figure 27. Schematic for Multi-Panel TPS Test Facility

was needed. Assuming that all other losses could be arrested, then 56% of the flow or 0.02 m<sup>3</sup>/sec (31 ft<sup>3</sup>/min) would be around and through the test specimen. Flow rates of this magnitude would have unrealistically heated the insulation, the support system, and the simulated vehicle structure and would have invalidated the test results.

Based on the considerations of high flow rate, the probability of success in sealing facility leaks, and the unpredictability of modification costs and schedule impact, a decision was made to discontinue the boost phase portion of the test cycle and all pressure loading of the test specimen during reentry. The final test profile is shown in figure 28.

Thermal-mechanical test results. - After completing the 50 reentry thermal cycles the specimen was in excellent condition as shown in figure 29. In the installed condition the panels were flat and free of local warpage or buckling. There was no evidence of problems associated with the thermal/structural design. Oxidation damage sites were observed; however, the majority of these had been sighted and documented during the test series. These were primarily related to conditions peculiar to the test or to manufacturing expediences and were not considered typical of flight hardware. In no instance did the damage compromise the ability of the structure to perform its design functions throughout the planned spectra of thermal and acoustic exposure. The oxidation damage was related to:

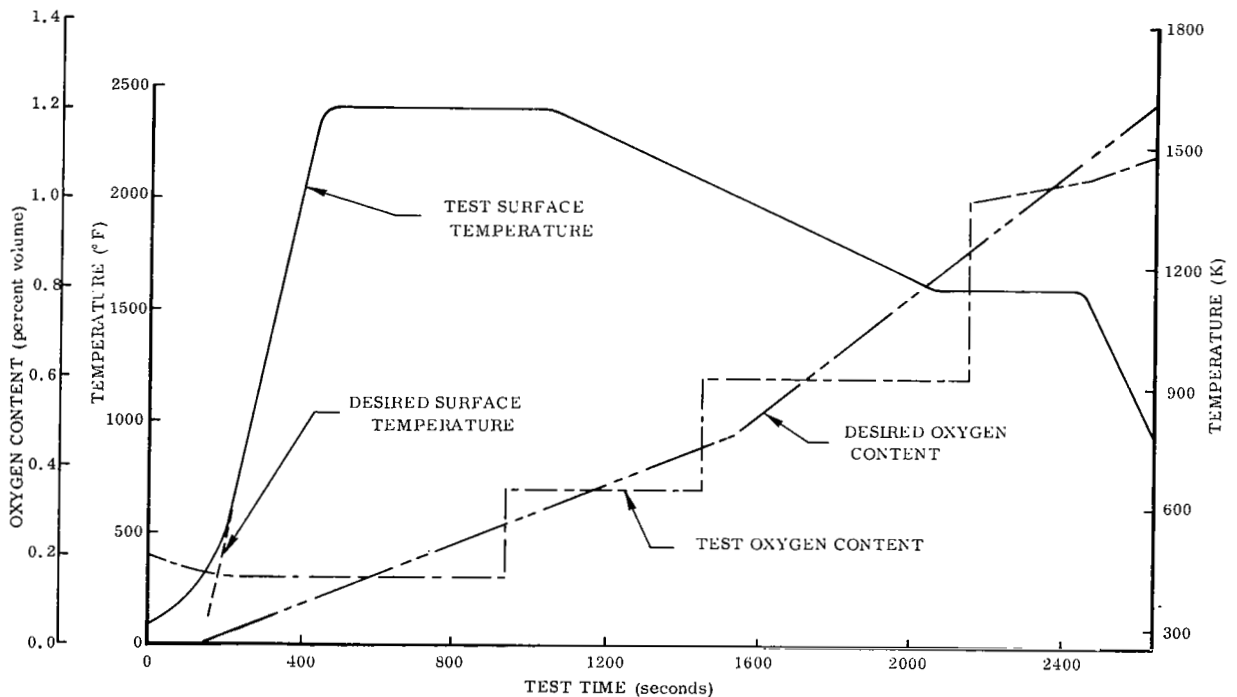


Figure 28. Test Parameters for Nine-Panel Test Specimen

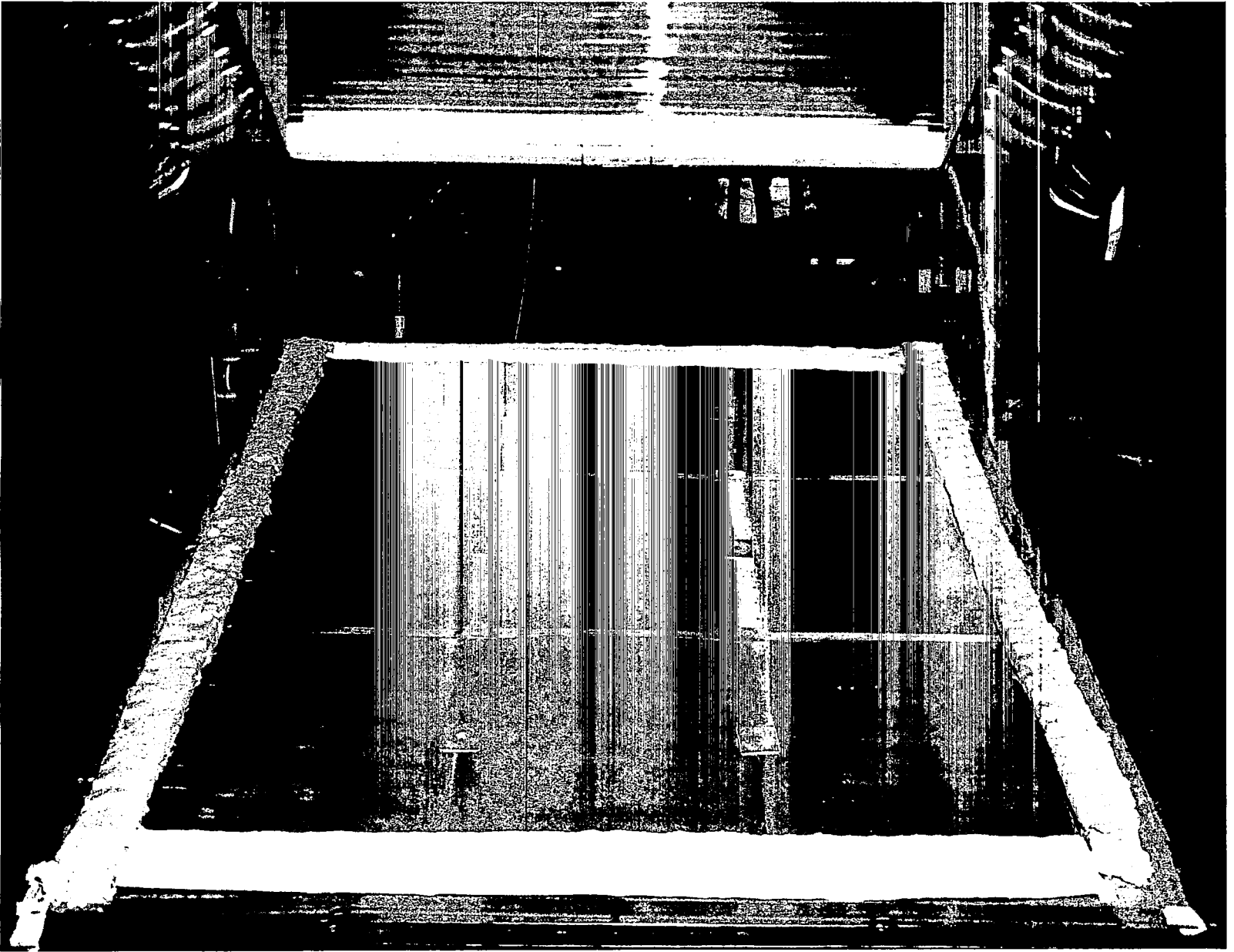


Figure 29. Nine-Panel TPS Specimen after 50 Cycles of Thermal Flight Simulation (Photo 13 8414)

(1) Design — where inadequate clearance was provided in the minor component re-design between Phase II (where no substrate oxidation was observed on any of the four specimens) and Phase III.

(2) Manufacturing — where a relaxation of quality control (such as for edge preparation, dimensionally incorrect parts, and an undetected crack) allowed normally unsatisfactory components to go into the assembly.

(3) Coating — where it is hypothesized that a non-uniform distribution of coating constituents contributed to premature oxidation.

(4) Incompatible materials — where the spring-loaded nickel alloy sheathed tungsten/rhenium thermocouple probes reacted with the silicide coating of the heat shields.

(5) Assembly — where coating damage in the form of chipping resulted from normal assembly and disassembly operations. In general the damage occurred in the hexagonal drive socket of the post filler plug, which was intended to be a non-reusable item.

In addition to these identifiable causes of substrate oxidation, some damage was sustained by the peripheral guard panels that resulted from severe thermal gradients between the panels and the water-cooled holding fixture. The physical damage occurred during disassembly by over-center flexing.

In summary, the vast majority of the oxidation sites were identifiable during normal inspection periods and without the aid of elaborate nondestructive evaluation techniques. The number of sites could have been substantially reduced by minor design improvements to reduce interferences and by improving manufacturing and coating quality control such as those employed during the small-size TPS fabrication.

Thermal correlation. — The average temperature measurements for the test series showed acceptable uniformity [4 K (8° F) to 13 K (22° F) at peak temperature] over the surface of the specimen. The average maximum temperature over the heat shield surfaces was 1587 K (2398° F) with the maximum temperature recorded at the specimen center of 1593 K (2408° F). The maximum recorded temperature was 1611 K (2440° F) which occurred during cycle 3.

Data plots of the average temperature history for four critical locations are shown in figure 30. The average maximum temperature at the center of the heat shield surface as recorded on the interior side was 1593 K (2408° F) compared to a programmed and predicted 1590 K (2400° F). The data closely followed the predicted curve until the final cool-down period after 2400 seconds from start of reentry. At this point the cool-down rate was slower than anticipated. This deviation was probably due to the heat stored in the Glasrock insulation above the lamps.

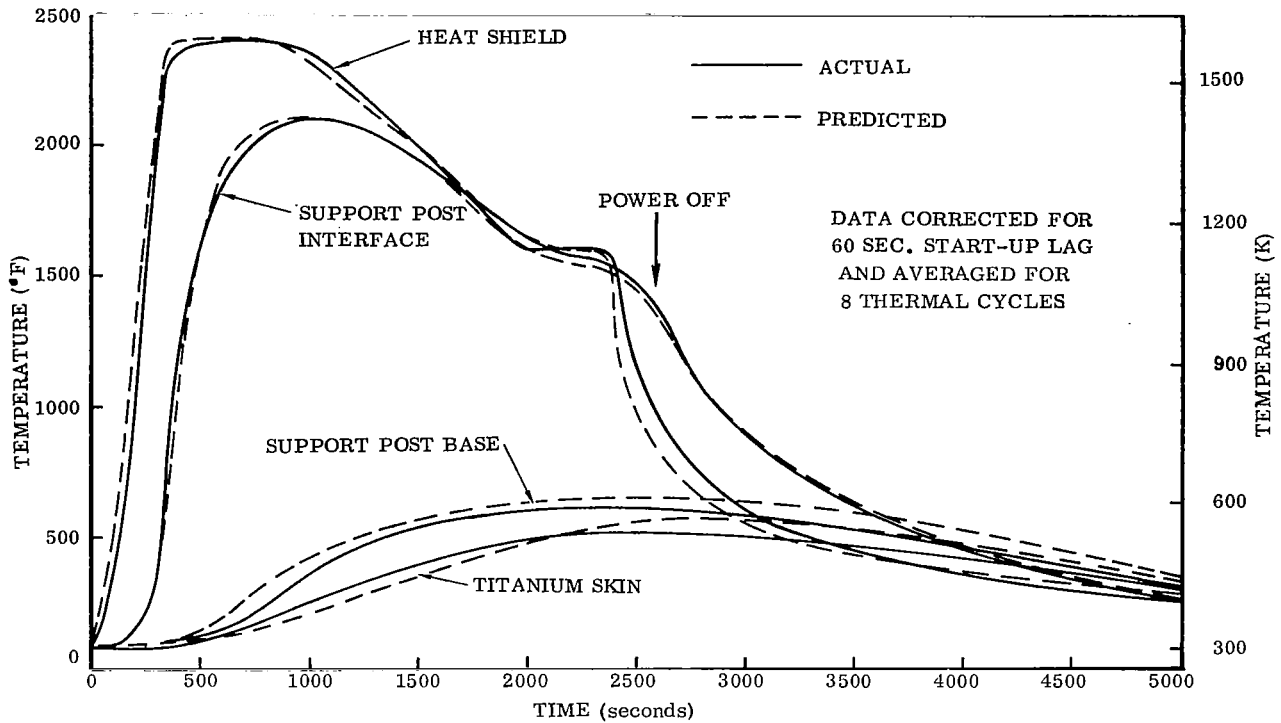


Figure 30. Radiant Heat Test Composite Temperature Distribution

The bi-metallic support post interface maximum temperature was 1419 K (2095° F) compared to a predicted level of 1422 K (2100° F). This data set exhibited excellent correlation over the entire recorded range with slight deviations occurring during the heat-up and during the simulated reentry maneuver (2000 to 2400 seconds following start of reentry).

The average maximum temperature at the base of the support post was 602 K (625° F) compared to a prediction of 616 K (650° F). The test data followed the predictions but were consistently lower. This was attributed to a possible difference in the thermal properties of HS-25, greater lateral thermal conductivity of Fiberfrax H than anticipated, and/or convective cooling air below the fixture.

Similarly, the titanium primary structure (consisting of skin, frames, and stiffeners) temperature data deviated from the predictions. The average maximum temperature was 547 K (525° F) compared with a prediction of 577 K (580° F). This could be the result of a variance in the thermal properties of Fiberfrax H, an error in the assumption of the thermal mass of the titanium structure, and/or convective cooling air below the fixture.

During thermal testing, opportunities arose that permitted investigation of refurbishment and repair of hardware for a typical thermal protection system. The earliest opportunity was presented at the end of thermal cycle 2 followed by local damage to the

hexagonal drive socket of the post filler plug after cycle 5. The damage after cycle 2 was determined to be test peculiar, arising from an apparent incompatibility of the thermocouple sheathing material, while under pressure in the test environment, with the silicide coating of the test hardware. The hexagonal socket damage was considered to be a normal condition for flight hardware resulting from mechanical coating damage during wrenching operations or improper edge preparation for coating. Both cases were allowed to grow unarrested. The thermocouple damage site was repaired after cycle 21 when it had grown to a 0.5 cm (0.2 inch) diameter hole. Wrenching damage was left unchecked for the complete test to assess the effect of uncontrolled oxidation on the removability of the plugs.

At the conclusion of thermal cycle 21, a damage site in the center test panel had progressed to a point requiring coating repair. Evidence of oxidation at this site was first noted at the end of cycle 12. This site was at the end of a skin to beam longitudinal weld where the weld bead had not been ground flush. During acoustic excitation the retainer strap had impacted the weld bead causing coating damage to both the retainer and the weld. Subsequent thermal cycling caused oxidation, material loss, and a small hole at the weld.

The damaged center panel was disassembled from the heat shield array, as planned for flight hardware, by removing six post filler plugs, four post retainer bolts (two others were only loosened), two center retainers, and two panel edge retainers. The panel was moved approximately 0.64 cm (0.25 inch) aft or downstream to clear it from its overlaying forward panel, then lifted out. The forward panel and the three adjacent panels were not disturbed or loosened to assist disassembly.

Three types of coating repair methods were attempted. In all cases the glass frit mixture [60 w/o-325 mesh Pyrex frit, 30 w/o-270 mesh alumina (flame spray grade), 10 w/o-325 mesh amorphous boron, mixed with a Microbraze vehicle] developed by McDonnell Douglas East (ref. 8) was applied generously to the oxidation site. All sites were prepared for repair coating by scraping or filing to remove the visible oxide and expose the base metal. The center heat shield was repaired under the best conditions, that is, in the laboratory, in a furnace. One of the guard panels was removed from the array but was repaired on-site. Other repairs were made with components in place.

The two panels that were field repaired (one on-site, one in-place) survived 10 additional thermal cycles when continued oxidation to the thermocouple damage sites indicated a need for a second repair. The same glass frit mixture repair coating was used, but the method of repair site preparation was changed. A Weller Minishop high speed (24 000 rpm) grinder was employed to remove the oxidized and contaminated material without removing either panel from the test array. All visual traces of the oxide were removed using a 0.31 cm (0.12 inch) diameter abrasive wheel. The repair material was applied as before but from one side only, and the repair site air dried at 535 K (500° F) while installed in the test facility. Fusing was then accomplished during the next thermal

cycle. The two repairs accomplished in this fashion protected the material from further oxidation throughout the remaining 19 test cycles. Examination of these panels after 50 thermal cycles showed that the two in-place field repairs made at cycle 31 protected the substrate and were well fused and glassy appearing for a minimum distance of 0.25 cm (0.10 inch) concentric to the hole, on both sides of each panel.

Post-thermal acoustic testing. - At the completion of thermal cycling, acoustic testing was resumed with cycles 51 through 100. Two post filler plugs, which were non-structural, failed during acoustic test and as a result of retorquing between test cycles. Post-test inspection showed no structural damage identifiable to acoustic excitation, no propagation of defects, and no unusual coating rubbing or scrubbing on mated surfaces. Inspection of the test specimen was performed initially every cycle and each fifth cycle after cycle 55. This inspection revealed that acoustic excitation was loosening the post retainer bolts, which were buried at the bottom of the retainer posts. Repeated retorquing to the established test level of 1.7 Nm (15 in-lb) did not solve the problem. After test cycle 66, all 10 post retainer bolts were tightened to a minimum of 2.8 to 3.4 Nm (25 to 30 in-lb) torque, solving the loosening problem during acoustic test. However, during final disassembly of the test specimen, removal torques were found to be as low as 0.6 Nm (5 in-lb), showing that the problem of fastener torquing or locking had not been resolved.

#### Test Evaluation

Specimen disassembly. - The center panel was disassembled from the array by removing the post filler plugs, unbolting the retainers, and sliding the panel from under the adjacent panel. Plugs that had been damaged by oxidation or torqued to failure did not delay removal of the submerged post retainer bolts. The remainder of disassembly was normal, excepting the removal of one post filler plug that had been permitted to oxidize so that no drive socket remained. This plug was drilled through and removed with an "Easyout" hand tool, a possibility that had been considered in design. During disassembly of the test specimen, one of the plugs was torqued to failure. Since the body of the plugs is cylindrical, access to the retainer bolt at the bottom of the post was still possible and the bolt was removed. All post retainer bolts were removed without difficulty, although the design would accommodate removal by "Easyout" tools if necessary. Disassembled heat shields and retainers after thermal and acoustic testing are shown in figure 31.

Thermal/structural performance. - Verification of the thermal design of the heat shield panels and justification for the selection of the nine-panel test array of heat shields were demonstrated by the results of the tests. The isolated center panel survived the full test spectrum with no thermal distortion or thermal stress failures. This panel experienced thermal and mechanical edge conditions that were representative of a typical heat shield on a flight vehicle. The flatness of the panel and the absence of distortion and thermal damage can be seen in figure 32. Considerable distortion occurred



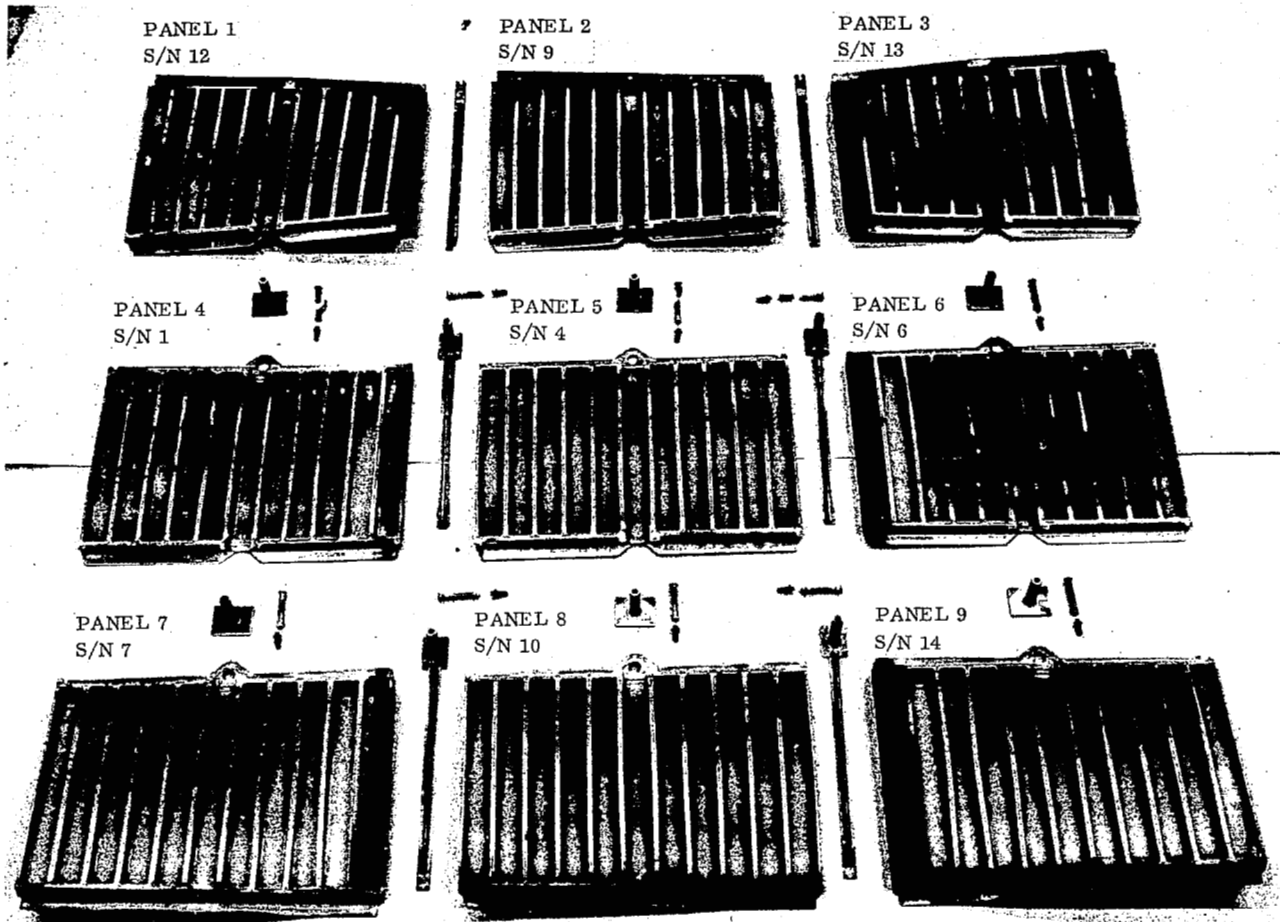


Figure 31. Disassembled Nine-Panel TPS Specimen Components After 50 Thermal and 100 Acoustic Life Cycle Tests (Photo 13 8756)



Figure 32. Panel After Testing (Photo 13 8714)

in the edge of guard panels making up the remainder of the nine-panel test array. These panels experienced severe thermal gradients unlike any to be encountered by flight hardware. The thermal gradients were created by the contact of these panels with the water-cooled frame of the holding fixture and caused thermal differentials in the order of 1370 K (2000° F) during thermal cycling.

Prior to fabrication of the holding fixture, it was predicted that the top flange of the support frame would experience temperatures in the order of 1366K (2000° F) and that the thermal gradients along the sides of the frame would not contribute to frame distortion since the frame was free to expand along its length. However, during the system checkout, the frame did distort excessively, necessitating the addition of frame side-member water-cooling tubes. However, design modifications were not made in the edge panels to accommodate the new thermal gradients existing between the heated panels and the water-cooled frame of the fixture. As a result, the edge panels all experienced warpage and thermal damage to some degree, and as expected, the four corner panels with two cool edges experienced more warpage and thermal stress damage than did the other four guard panels that had only one cool edge.

In retrospect, it would have been preferable to have more thoroughly analyzed the relationship between the water-cooled frame and the edge panels. This would have shown the necessity for isolating the edge panels from the frame by using guard panels such as were successfully employed in the Phase II test specimens. (The guard panels, although originally planned for the Phase III specimen, were eliminated in an effort to reduce the number of components and to ease the specimen assembly.) However, it is reiterated that the thermal conditions of the peripheral heat shields that existed during the Phase III test series were significantly different from those predicted for vehicle flight. All panels should be expected to perform similarly to the central test panel; that is, free of thermal distortion and thermal stress failures. The history of this program, both Phases II and III, showed that when properly isolated from the thermal abnormalities of the test frame, the panels will not experience any thermal/structural failures.

#### TPS WEIGHT ASSESSMENT

Slight modifications were made to the TPS components between phases I and II, but the major weight reduction resulted from the change of insulation materials. The various panel configuration system component weights are given in table VII.

The resulting unit weight of the metallic components before coating was 12.05 kg/m<sup>2</sup> (2.47 lb/ft<sup>2</sup>). After coating the unit weight increased to 12.98 kg/m<sup>2</sup> (2.66 lb/ft<sup>2</sup>). Using 113.7 kg/m<sup>3</sup> (7.1 lb/ft<sup>3</sup>) density Fiberfrax H, the insulation unit weight was 10.83 kg/m<sup>2</sup> (2.22 lb/ft<sup>2</sup>). This resulted in a total system unit weight of 23.81 kg/m<sup>2</sup> (4.88 lb/ft<sup>2</sup>) in the as-coated condition. This compares to 28.06 kg/m<sup>2</sup> (5.75 lb/ft<sup>2</sup>) for the tee-stiffened fabricated during Phase II and represents a unit weight reduction of 18%.

TABLE VII  
TPS WEIGHT SUMMARY

Configuration System	Unit Weight			
	Metallic Components		Insulation	Total System
	Before Coating	After Coating		
Phase II Tee Stiffened	11.91 kg/m <sup>2</sup> (2.44 lb/ft <sup>2</sup> )	13.03 kg/m <sup>2</sup> (2.67 lb/ft <sup>2</sup> )	15.03 kg/m <sup>2</sup> (3.08 lb/ft <sup>2</sup> )	28.06 kg/m <sup>2</sup> (5.75 lb/ft <sup>2</sup> )
Phase II Open Corrugation	12.69 kg/m <sup>2</sup> (2.60 lb/ft <sup>2</sup> )	13.43 kg/m <sup>2</sup> (2.75 lb/ft <sup>2</sup> )	15.03 kg/m <sup>2</sup> (3.08 lb/ft <sup>2</sup> )	28.45 kg/m <sup>2</sup> (5.83 lb/ft <sup>2</sup> )
Phase III Tee Stiffened (as tested)	12.05 kg/m <sup>2</sup> (2.47 lb/ft <sup>2</sup> )	12.98 kg/m <sup>2</sup> (2.66 lb/ft <sup>2</sup> )	10.83 kg/m <sup>2</sup> (2.22 lb/ft <sup>2</sup> )	23.81 kg/m <sup>2</sup> (4.88 lb/ft <sup>2</sup> )
Final System (with optimized insulation and support posts)	11.96 kg/m <sup>2</sup> (2.45 lb/ft <sup>2</sup> )	12.88 kg/m <sup>2</sup> (2.64 lb/ft <sup>2</sup> )	10.10 kg/m <sup>2</sup> (2.07 lb/ft <sup>2</sup> )	22.98 kg/m <sup>2</sup> (4.71 lb/ft <sup>2</sup> )

The most significant contribution to the weight reduction was attributed to the employment of a lower density fibrous insulation. That is, the nominal 96 kg/m<sup>3</sup> (6.0 lb/ft<sup>3</sup>) density Fiberfrax H compressed to 113.7 kg/m<sup>3</sup> (7.1 lb/ft<sup>3</sup>) replaced 160 kg/m<sup>3</sup> (10 lb/ft<sup>3</sup>) Dyna-Flex compressed to 192 kg/m<sup>3</sup> (12 lb/ft<sup>3</sup>). Since the Fiberfrax H was more thermally efficient (i.e., a lower thermal conductivity-density product) the insulation thickness could have been reduced from 9.4 cm (3.7 inches) to 8.6 cm (3.4 inches). With the corresponding reduction in support post height, the resulting TPS unit weight would be 22.98 kg/m<sup>2</sup> (4.71 lb/ft<sup>2</sup>) of which the insulation contributes 10.10 kg/m<sup>2</sup> (2.07 lb/ft<sup>2</sup>). This, therefore, should be considered the final system weight.

#### TPS COST ASSESSMENT

Since the small-size TPS fabrication effort revealed that the highest cost and most uncontrollable item was the raw material, the subsequent design/fabrication functions endeavored to reduce the amount of material utilized. This was accomplished by increasing the man-related operations such as welding and machining. As shown in table VIII, the material cost was reduced by 70%. The man-related functions show an appropriate percentage increase, but the overall cost was reduced by 21%.

The cost data presented is based on the actual fabrication expenses for 16 heat shields and their appropriate support components. This represents an area of approximately 2 m<sup>2</sup> (21.3 ft<sup>2</sup>) or approximately two-thirds of the estimated applicable area of the baseline vehicle. The costs include raw material, machining, forming, finishing, joining, and coating.

TABLE VIII

FINAL TPS FABRICATION PROCESS  
PERCENTAGE COST BREAKDOWN

Item	Percent of Total Cost	
	Phase III	Phase II
Material	10.3	34.2
Machining	41.2	31.1
Forming/Finishing	7.8	5.8
Welding	15.1	11.3
Coating	25.4	17.4
Brazing	0.2	0.2

The cost of the components (including heat shield, support system, and insulation) was \$1100/kg (\$500/lb). This compares with the \$1140/kg (\$518/lb) cost for the tee-stiffened TPS components fabricated during Phase II. Both the total system cost and unit weight were reduced during Phase III resulting in a net cost/weight saving of approximately 4%.

The individual component cost data was compiled into an nth unit format and the costs projected for five Orbiter vehicles. The assumptions were: that 24

heat shield units would be required per vehicle; the current actual costs were baseline; there would be no reduction in per pound material cost; and there would be approximately an 89% composite learning factor (ref.11) applied to all fabrication parameters. This composite was based on the assumptions that learning factors were 100% for material; 90% for machining, joining, and coating; and 85% for forming and finishing. The cumulative average cost for n units is shown in figure 33. In addition to the Phase III components cost projections, those generated during Phase II are also shown for comparison. The variation in the curves is due to the initial cost since the same learning curve factors at an 89% slope were applied.

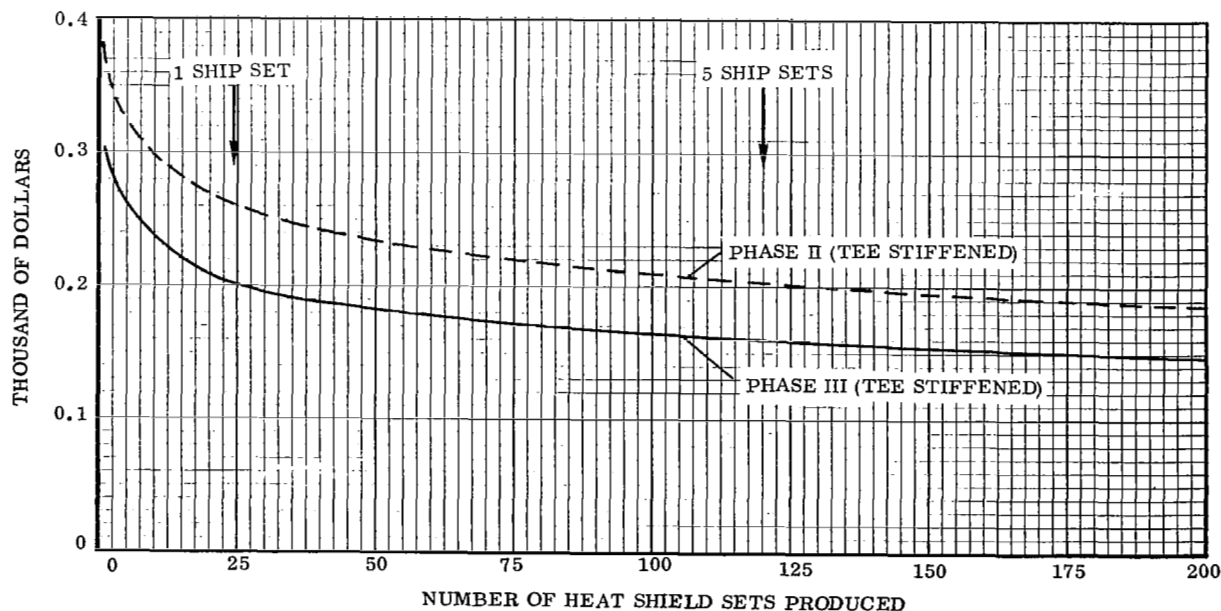


Figure 33. Tee-Stiffened TPS Cumulative Average Cost

In interpreting the data in figure 33 it can be seen that for the selected system one ship set of 24 heat shields, components, and insulation covering an area of 3 m<sup>2</sup> (32 ft<sup>2</sup>), the cumulative cost would be \$49 870. This relates to approximately \$750/kg (\$340/lb). Similarly, for five ship sets of 120 heat shields and components the cumulative cost would be \$193 520 or \$580/kg (\$265/lb).

### CONCLUDING REMARKS

The intent of this program was to prove the feasibility of and to develop a flight-worthy thermal protection system fabricated from a columbium alloy material system. The program evolution proceeded from establishing criteria, characterizing the candidate material systems, determining or verifying mechanical property data, evaluating by fabrication and test elemental, subsize, and small size TPS configurations, to finally subjecting a full size, multi-panel TPS array to representative flight thermal and acoustical conditions.

Of the six material systems evaluated, Cb-752 coated with R-512E was found to be the most durable and consistently the best system. Cb-752 and C-129Y were very similar in forming and joining characteristics. WC-3015 was found to be the most weldable but the least coatable, the latter due to an increase in the ductile-to-brittle transition temperature associated with the coating process and annealing. WC-3015 also suffered from delamination and it was determined, therefore, that the material was not acceptable sheet quality at this stage of its development. Of the two coatings evaluated R-512E was found to be consistent in quality and endurance, while VH-109 was found to suffer from quality control. However, all systems sustained a minimum of 42 simulated flight thermal and load cycles and exhibited considerable damage tolerance. The R-512E coating performed very well with a survivability mean of 99.9 cycles for 44 elemental specimens. A total of 7124 cycles was sustained by all of the elemental specimens.

Distinct differences were found between cyclic creep measurements made throughout the flight simulation testing and standard isothermal creep. Considerable creep testing and metallurgical studies are needed to resolve inconsistencies and to develop truly representative cyclic creep data.

Environmental testing through 100 thermal and mechanical load cycles of the subsize heat shields confirmed the structural adequacy of the two configurations. Ten panels were subjected to flight simulation exposure and received a combined total of 964 cycles with all but one panel completing the targeted 100 cycles. Of the two material systems evaluated, Cb-752/R-512E performed better than C-129Y/R-512E. No structural failures of either system resulted from the testing although severe substrate erosion occurred on the C-129Y/R-512E tee-stiffened panels. Field repair techniques were also evaluated during the subsize heat shield testing. Areas of coating degradation and/or substrate

oxidation were clearly identifiable, thereby enabling a component to be removed and repaired. Repaired areas that were properly prepared by removing the contaminated region were proven completely successful after continued cycling.

The effects of lightning strikes on coated columbium alloy heat shields had not been defined prior to the initiation of this program. It was anticipated that the non-conductive silicide coating could accentuate problems with electrical bonding and intrastructural arcing. From a series of tests employing simulated heat shields and supports it was concluded that (1) although some local damage was possible the TPS could withstand a typical cloud-to-cloud discharge without perforation, and (2) maximum current strike, typical of a cloud-to-ground strike, would cause extensive damage. In the latter case, however, the damaged area would be clearly identifiable before launch, thereby enabling component repair or replacement. Although a strike to the vehicle is considered a small probability, a typical strike would be one swept from the nose to the tail producing pit marks and occasional small holes but would not jeopardize the mission due to structural failure.

Impact tests simulating a micrometeoroid environment were also conducted. These tests consisted of microparticle erosion, small particle cratering, and penetration. Test velocities ranged up to 15 km/sec. The tests were conducted on coated specimens without thermal exposure and on those having 50 thermal cycles. No coating or substrate damage was observed as a result of either the erosion or cratering conditions. The perforated specimens were repaired by field repair techniques and subsequently successfully cycled 50 times through a simulated entry temperature profile.

The tee-stiffened and open corrugation heat shield configurations evaluated as sub-size panels were designed into small-size, full-scale TPS models that included split bi-metal support posts, retainers, close-outs, and insulation. The fabrication processes used in fabricating four models (two of each configuration) included machining, sheet metal forming, electrical discharge machining, welding, brazing, heat treating, and creep flattening. All were employed without difficulty and resulted in high quality components. Electron beam welding was demonstrated to be highly flexible and versatile. This permitted the economical weld fabrication of many articles of hardware heretofore considered impractical and too expensive. The extremely high and local input energy levels inherent to electron beam welding permitted the use of minimum tooling and resulted in few weld distortion problems.

Two types of thermal testing were conducted on each small-size configuration. The first test was intended to investigate structural integrity and system leakage effects under convective hot gas flow. The second test involved the simultaneous exposure of temperature, local surface pressure, and pressure differential loading. In addition, all specimens were exposed to acoustic excitation at levels up to 155 dB simulating 100 missions.

Each specimen that was exposed to 20 hot gas flow cycles in a one atmosphere oxidizing environment experienced no substrate oxidation or structural degradation. The open corrugation TPS, however, did suffer a braze disbond between the skin and a transverse beam. This condition was attributed to a combination of substandard braze diffusion and an improperly assembled specimen.

Two specimens were also exposed to 50 cycle radiant heat profiles. These specimens exhibited no structural degradation or coating failure. All systems responded well to the thermal environments and the temperature distributions were within close tolerances of the predicted levels. No disruption or deterioration of the insulation was found after any of the tests. All systems were able to be disassembled as required between cycles and at the conclusion of the test series. Based on the overall weight and fabrication costs plus the relative test performance, the tee-stiffened TPS was selected for the final multi-panel TPS evaluation.

The flight-size, full-scale metallic thermal protection system in a nine-panel array performed most capably and proved to be not only reusable but also rugged and durable and possessed a high degree of damage tolerance. The heat shield surface hardware (i. e., heat shield panels and panel retainers) remained flat and free of undesirable distortion throughout testing, thereby validating thermal/structural design and analysis. The blanket insulation performed efficiently with no evidence of degradation due to thermal cycling, vibration, or environmental moisture.

Disassembly and reassembly of individual heat shields, simulating interflight removal from flight vehicles, was demonstrated between test cycles and at the end of simulated reentry flights. Refurbishment and repair of TPS hardware was accomplished, when needed, following disassembly from the array, and with the hardware in-place in the specimen. Properly applied repair coatings displayed good life expectancy.

Coated columbium alloy filler plugs and superalloy panel retainer bolts were readily removed by conventional means both between test cycles and at the completion of testing. As anticipated in design, the expendable retainer bolts and plugs were removable with "Easyout" tools when damage precluded the use of conventional tools.

In conclusion, it is believed that a reusable and structurally reliable TPS consisting of a combination of columbium alloy components, superalloy components, and fibrous blanket insulation, weighing less than  $23 \text{ kg/m}^2$  ( $5 \text{ lb/ft}^2$ ) has been demonstrated to be state-of-the-art for Space Shuttle type vehicle service.

Convair Division of General Dynamics,  
San Diego, California, March 12, 1975.

## APPENDIX A

### CONVERSION OF U.S. CUSTOMARY UNITS TO SI UNITS

The International System of Units (designated SI) was adopted by the Eleventh General Conference on Weights and Measures in 1960. The units and conversion factors used in this report are taken from or based on NASA SP-7012, "The International System of Units, Physical Constants and Conversion Factors — Revised, 1969".

The following table expresses the definitions of miscellaneous units of measure as exact numerical multiples of coherent SI units, and provides multiplying factors for converting numbers and miscellaneous units to corresponding new numbers of SI units.

The first two digits of each numerical entry represent a power of 10. An asterisk follows each number that expresses an exact definition. For example, the entry "-02 2.54\*" expresses the fact that 1 inch =  $2.54 \times 10^{-2}$  meter, exactly, by definition. Most of the definitions are extracted from National Bureau of Standards documents. Numbers not followed by an asterisk are only approximate representations of definitions, or are the results of physical measurements.

#### ALPHABETICAL LISTING

<u>To convert from</u>	<u>to</u>	<u>multiply by</u>	
atmosphere (atm)	newtons/meter <sup>2</sup> (N/m <sup>2</sup> )	+05	1.0133*
British thermal unit, mean (Btu)	joule (J)	+03	1.056
Fahrenheit (F)	kelvin (K)	$t_k = (5/9)(t_f + 459.67)$	
foot (ft)	meter (m)	-01	3.048*
inch (in.)	meter (m)	-02	2.54*
mil	meter (m)	-05	2.54*
millimeter of mercury (mm Hg)	newton/meter <sup>2</sup> (N/m <sup>2</sup> )	+02	1.333
nautical mile, U.S. (n.mi.)	meter (m)	+03	1.852*



APPENDIX A — Continued

<u>To convert from</u>	<u>to</u>	<u>multiply by</u>	
pound force (lb <sub>f</sub> )	newton (N)	+00	4.448*
pound mass (lb <sub>m</sub> )	kilogram (kg)	-01	4.536*
torr	newton/meter <sup>2</sup> (N/m <sup>2</sup> )	+02	1.333

PHYSICAL QUANTITY LISTING

<u>Acceleration</u>			
foot/second <sup>2</sup> (ft/sec <sup>2</sup> )	meter/second <sup>2</sup> (m/sec <sup>2</sup> )	-01	3.048*

<u>Area</u>			
foot <sup>2</sup> (ft <sup>2</sup> )	meter <sup>2</sup> (m <sup>2</sup> )	-02	9.290*
inch <sup>2</sup> (in <sup>2</sup> )	meter <sup>2</sup> (m <sup>2</sup> )	-04	6.452*
inch <sup>2</sup> (in <sup>2</sup> )	centimeter <sup>2</sup> (cm <sup>2</sup> )	+00	6.452

<u>Density</u>			
pound mass/foot <sup>3</sup> (pcf, lb <sub>m</sub> /ft <sup>3</sup> )	kilogram/meter <sup>3</sup> (kg/m <sup>3</sup> )	+01	1.602
pound mass/inch <sup>3</sup> (lb <sub>m</sub> /in <sup>3</sup> )	kilogram/meter <sup>3</sup> (kg/m <sup>3</sup> )	+04	2.768
pound mass/inch <sup>3</sup> (lb <sub>m</sub> /in <sup>3</sup> )	gram/centimeter <sup>3</sup> (g/cm <sup>3</sup> )	+01	2.768

<u>Energy</u>			
British thermal unit, mean (Btu)	joule (J)	+03	1.056

<u>Energy/Area Time</u>			
Btu/foot <sup>2</sup> second (Btu/ft <sup>2</sup> sec)	watt/meter <sup>2</sup> (W/m <sup>2</sup> )	+04	1.135

<u>Force</u>			
kilogram force (kg <sub>f</sub> )	newton (N)	+00	9.807*
pound force (lb <sub>f</sub> )	newton (N)	+00	4.448*

APPENDIX A — Continued

<u>To convert from</u>	<u>to</u>	<u>multiply by</u>	
<u>Length</u>			
foot (ft)	meter (m)	-01	3.048*
inch (in.)	meter (m)	-02	2.54*
micron	meter (m)	-06	1.00*
mil	meter (m)	-05	2.54*
mile, U.S. nautical (n.mi.)	meter (m)	+03	1.852*
<u>Mass</u>			
pound mass (lb <sub>m</sub> )	kilogram (kg)	-01	4.536*
<u>Pressure</u>			
atmosphere (atm)	newton/meter <sup>2</sup> (N/m <sup>2</sup> )	+05	1.013*
millimeter of mercury (mm Hg)	newton/meter <sup>2</sup> (N/m <sup>2</sup> )	+02	1.333
pound/foot <sup>2</sup> (psf, lb <sub>f</sub> /ft <sup>2</sup> )	newton/meter <sup>2</sup> (N/m <sup>2</sup> )	+01	4.788
pound/inch <sup>2</sup> (psi, lb <sub>f</sub> /in <sup>2</sup> )	newton/meter <sup>2</sup> (N/m <sup>2</sup> )	+03	6.895
<u>Temperature</u>			
Fahrenheit (F)	Kelvin (K)	$t_k = (5/9) (t_f + 459.67)$	
<u>Volume</u>			
foot <sup>3</sup> (ft <sup>3</sup> )	meter <sup>3</sup> (m <sup>3</sup> )	-02	2.832*
inch <sup>3</sup> (in <sup>3</sup> )	meter <sup>3</sup> (m <sup>3</sup> )	-05	1.639*
inch <sup>3</sup> (in <sup>3</sup> )	centimeter <sup>3</sup> (cm <sup>3</sup> , cc)	-01	1.639

APPENDIX A — Concluded

PREFIXES

The names of multiples and submultiples of SI units may be formed by application of the prefixes:

Multiple	Prefix
$10^{-6}$	micro ( $\mu$ )
$10^{-3}$	milli (m)
$10^{-2}$	centi (c)
$10^{-1}$	deci (d)
$10^3$	kilo (k)
$10^6$	mega (M)
$10^9$	giga (G)

## REFERENCES

1. Black, W. E.; et al.: Evaluation of Coated Columbium Alloy Heat Shields for Space Shuttle Thermal Protection System Application, Vol. I, Phase I — Environmental Criteria and Material Characterization. NASA CR-112119, June 1972.
2. Black, W. E.; et al.: Evaluation of Coated Columbium Alloy Heat Shields for Space Shuttle Thermal Protection System Application, Vol. II, Phase II — Subsize Heat Shield and Small Size TPS Evaluation. NASA CR-112119-2, Aug. 1973.
3. Baer, J. W.; and Black, W. E.: Evaluation of Coated Columbium Alloy Heat Shields for Space Shuttle Thermal Protection System Application, Vol. III, Phase III — Full Size TPS Evaluation. NASA CR-112119-3, Mar. 1974.
4. Stein, B. A.; Rummeler, D. R.; and Jackson, L. R.: Refractory Metal Heat Shield Technology for Space Shuttle. Paper presented at NASA Space Shuttle Technology Conference, Lewis Research Center (Cleveland, Ohio), July 15-17, 1970.
5. Davis, J. W.; and Fitzgerald, B. G.: Fused Slurry Silicide Coatings for Columbium Alloy Reentry Heat Shields. Third Quarterly Technical Progress Narrative, McDonnell Douglas Astronautics Company — East, May 14, 1971.
6. Favor, R. J.; Maykuth, D. J.; Bartlett, E. S.; and Mindlin, H.: Determination of Design Allowable Strength Properties of Elevated-Temperature Alloys, Part 1 — Coated Columbium Alloys. Contract NAS8-26325, Battelle Columbus Laboratories, Mar. 31, 1972.
7. Richardson, A. J.; and Sanders, J. P.: Discrete Particle Penetration Mechanics Based on Debris Particles of Two Materials, North American Rockwell Space Division Report SD70-463, Oct. 1971.
8. Culp, J. D.: Field Repair of Coated Columbium Thermal Protection Systems (TPS). MDC E0681, Contract NAS8-26121, McDonnell Douglas Astronautics Co. — East, Sep. 15, 1972.
9. Bartlett, E. S.; et al.: Degradation of Reuse of Radiative-Thermal-Protection-System Materials for the Space Shuttle. DCN 1-1-50-13647 (1F), Contract NAS8-26205, Battelle Columbus Laboratories, Oct. 25, 1972. (NASA CR-123587, 1971)
10. Freedman, A. H.; and Mikus, E. B.: High Remelt Temperature Brazing of Columbium Honeycomb Structures. Supplement to The Welding Journal, June 1966.
11. Boren, H. E.; and Campbell, H. G.: Learning Curve Tables, Vol. II, 86-99 Percent Slopes. RM-6191-PR Vol. III, The Rand Corporation, Apr. 1970.